INEEL/EXT-99-00459

Equal Channel Angular Extrusion

Progress Report for March 1998-May 1999

October 1999

Idaho National Engineering and Environmental Laboratory
Bechtel BWXT Idaho, LLC

INEEL/EXT-99-00459

Equal Channel Angular Extrusion
Progress Report for March 1998–May 1999

Contributors

Idaho National Engineering and Environmental Laboratory
- Jenya Macheret
- Gary E. Korth
- Thomas M. Lillo
- Arthur D. Watkins
- John E. Flinn, University of Idaho

Pacific Northwest National Laboratory
- Darrell R. Herling
- Mark T. Smith

Los Alamos National Laboratory
- Ricardo B. Scwarz

Published October 1999

Idaho National Engineering and Environmental Laboratory
Idaho Falls, Idaho 83415

Prepared for the
U.S. Department of Energy
Assistant Secretary for
Environmental Management
Under DOE Idaho Operations Office
Contract DE-AC07-99ID13727

ABSTRACT

Pure copper and Alloy 5083 aluminum were processed by equal channel angular extrusion (ECAE); their microstructural evolution and corresponding mechanical properties were investigated. Work also began on the possible use of ECAE to synthesize advanced materials or to consolidate metal powders or powder mixtures.

The die tooling used for ECAE is described and selected microstructural and mechanical property results for ECAE-processed copper and cold-rolled (conventionally-processed) copper in the as-processed and annealed condition are compared. Results thus far show that the "pure" metal is prone to low temperature recrystallization after large strain hardening—more beneficial effects are expected in the dispersion-strengthened and precipitation-hardening alloys. The large range of tensile properties and grain sizes from the copper allowed a flow stress analysis to be performed. From this analysis, a new model for flow stress behavior is proposed.

An evaluation of ECAE processing of material for spot welding electrodes began. Results to date include electrodes of ECAE-processed commercially pure copper (Alloy 101). Future work involving Glidcop® (Al_2O_3 oxide dispersion-strengthened copper) and CuCrZr (Cr-Zr precipitation dispersion) materials will be required to fully investigate the benefits of ECAE for electrode life extension.

Initial work on Aluminum Alloy 5083 showed that ECAE led to grain refinement as well as broke up and more uniformly dispersed the hardening precipitates. This is desirable for enhancing superplastic behavior.

Study of ECAE for consolidating metal powder began. Early results with a Cu-Ag powder indicate that near 100% density was achieved with room-temperature consolidation.

SUMMARY

This program is evaluating the potential of a novel metals processing technique called equal channel angular extrusion (ECAE) for developing advanced industrial materials for the transportation industry. The program is a collaborative effort among three national laboratories, the Idaho National Engineering and Environmental Laboratory (INEEL), Pacific Northwest National Laboratory (PNNL), and Los Alamos National Laboratory (LANL). The program began in March 1998; this report describes progress through May 1999.

INEEL is performing ECAE on a variety of materials and investigating their microstructural evolution and mechanical properties. Pure copper was chosen for the initial stage of the investigation because the extensive data on the microstructure and properties of copper in the literature allow a thorough comparative study of ECAE vs. conventional processing. Also, dispersion-strengthened copper alloys are widely used in industry. In particular, these alloys are used in the transportation industry for manufacturing spot welding electrodes. Evaluation of ECAE of copper and its alloys could, therefore, lead to developing improved materials for important industrial applications.

PNNL is investigating the effect of ECAE on the grain size of aluminum Alloy 5083. It is hypothesized that ECAE will refine the grain size and enhance the alloy's superplasticity. Samples were sent to INEEL for ECAE and returned to PNNL for characterization.

LANL is investigating ECAE as a means of synthesizing advanced materials by consolidating metal powders or powder mixtures such as metal matrix composites and immiscible elemental and amorphous metallic powders.

Initially, an ECAE die was borrowed from ALCOA. Subsequently, a new ECAE die was designed and fabricated. The work on copper has shown that ECAE and subsequent recrystallization result in microstructures with a large fraction (close to theoretical) of twin grain boundaries. These boundaries are believed to play an important role in the initiation of plastic flow. The flow stress analysis of the tensile behavior of these materials has shown that stress vs. strain behavior can be explained by a general framework of dislocation strengthening mechanisms. Further work is planned with aluminum, brass (Cu-30Zn), and nickel to see if ECAE has the same effect on these metals.

Spot welding electrodes made from ECAE commercially-pure copper (Alloy 101) did not perform better than conventionally processed material. This behavior can be explained by early recrystallization and subsequent grain growth of the ECAE materials. It is expected, however, that Glidcop® (Al_2O_3 oxide dispersion strengthened copper) and CuCrZr (Cr-Zr precipitation dispersion) materials will be thermally stable after ECAE due to pinning effects of the dispersion phase on the grain boundaries. These materials will be processed to investigate the benefits of ECAE on electrode life.

Initial work on aluminum Alloy 5083 (both commercial and Mn- or Zr-modified) at PNNL showed that grain refinement and breakup and more uniform dispersion of hardening precipitates was achieved by ECAE. These are desirable

to enhance superplastic behavior. Additional Alloy 5083 samples will be processed with different ECAE parameters to explore the superplasticity potential of this alloy.

Initial results from LANL for a Cu-Ag powder consolidated using ECAE indicate that near 100% density was achieved with room temperature consolidation. Thus ECAE may be useful for consolidating metallic powders at temperatures below those currently used. This study will continue to pursue consolidation of various elemental and/or alloy powders and powder mixtures, most likely including magnetic and amorphous powders.

FOREWORD

This equal channel angular extrusion research is a joint effort of three U.S. Department of Energy laboratories, the Idaho National Engineering and Environmental Laboratory, Pacific Northwest National Laboratory, and Los Alamos National Laboratory. This report covers work performed from March 1998 to May 1999; future progress reports will give further results.

ACKNOWLEDGMENTS

This work is supported by the U. S. Department of Energy's Office of Transportation Technologies (Office of Heavy Vehicle Technologies) under the direction of Dr. Sid Diamond. Acknowledgment is given to Vladmir Segal, the inventor of Equal Channel Angular Extrusion, which was developed in the previous USSR and has the potential of enabling the synthesis of materials with unique microstructures and thus unique mechanical properties. The contribution of Dr. Diamond is gratefully acknowledged; he recognized the potential of this novel extrusion technique and put together a team of researchers from several DOE national laboratories and Dr. Segal and provided a lot of enthusiasm for investigating possible applications of this unique processing method.

CONTENTS

FIGURES

TABLES

Equal Channel Angular Extrusion
Progress Report for March 1998–May 1999

1. INTRODUCTION

This program is investigating a novel metals processing technique called equal channel angular extrusion (ECAE) and evaluating its potential for developing advanced industrial materials for the transportation industry.

1.1 Description of ECAE

There exists a variety of methods to impose large plastic strains on materials in order to produce fine-grained microstructures. Forging, extrusion, drawing, and rolling have been used for this purpose, but they all have significant drawbacks. Multiple reductions of the initial billet cross-section are limited by the geometrical change of the work piece, require high loads, and result in a nonuniform deformation. In rolling, for example, the strain levels needed to achieve the formation of ultra-fine grain structures are only reached in thin foils. These problems pose significant limitations for production of larger parts or synthesis and processing of new materials with the objective of developing special microstructures and properties.

Many limitations associated with the conventional metal deformation techniques can be overcome by ECAE, a method was developed and patented in the former Soviet Union.[1] The benefits of ECAE come from its ability to impose intense simple shear deformation through innovative die design. Unlike conventional extrusion processes, the cross-section of billets extruded via ECAE is not reduced. This process, therefore, can be applied repeatedly through multi-pass operations to achieve strains of significant magnitudes while preserving the billet size. Each consecutive pass through a 90-degree die arrangement increases the strain intensity by 1.15. Table 1 lists the effective strain intensity and equivalent reduction for multiple passes. There is no geometric restriction on the strain magnitude that can be achieved. It has been shown that four or more passes creates a homogeneous and stable microstructure.[2] In addition, by choosing appropriate billet orientations as it enters the extrusion die on each pass, a variety of microstructures and textures can be developed. ECAE, therefore, has a potential to emerge as an important metal processing method for obtaining ultra-fine grain structures in alloys in bulk forms. Figure 1 illustrates the ECAE process.

Table 1. Effective strain intensity and equivalent reductions.

Number of Passes	Total Strain Intensity	Equivalent Area Reduction (%)	Equivalent Reduction Ratio (x:1)
1	1.15	69	3
2	2.31	90	10
3	3.46	97	33
4	4.62	99	105
5	5.77	99.7	335
6	6.93	99.9	1073
7	8.09	99.97	3436
8	9.24	99.99	10100

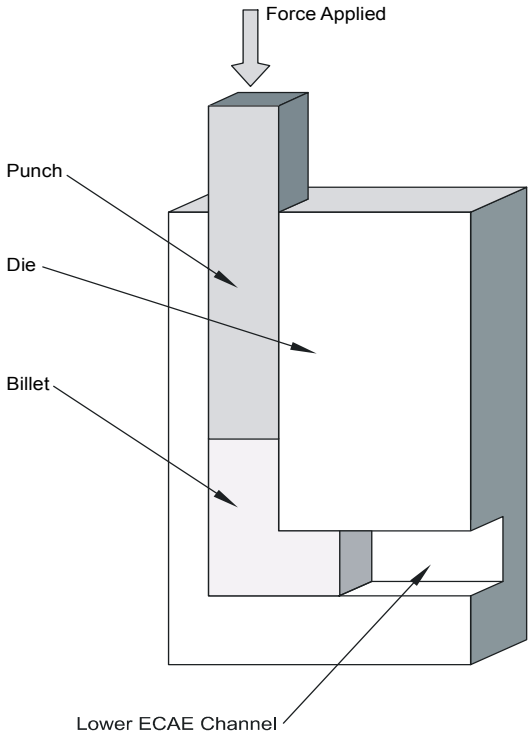

Figure 1. Cutaway of the ECAE die showing the extrusion process.

1.2 Purpose and Scope of This Investigation

Many unanswered questions remain regarding the nature and thermal stability of grains produced by severe plastic deformation. Systematic studies are needed to investigate microstructural evolution, stability, and grain growth under controlled thermal exposures as well as corresponding mechanical properties of the processed materials.

It is well known that large deformation results in microstructures with small grains and extensive dislocation cells development, often leading to corresponding increases in strength. In two-phase materials based on copper, the fine grains in the copper matrix may provide strengthening, while the second phase in the form of fine precipitates may pin the grain boundaries and improve thermal stability. These materials should potentially be attractive for high strength and high thermal/electrical conductivity applications, such as, for example, electrodes used for resistance welding of automotive structures. During service, the electrodes exhibit degradation due to electrode tip deformation (commonly referred to as “elephant foot”). In this investigation, a systematic study of the effect of ECAE processing on possible extension of the electrode life performance was undertaken.

As is often observed, the fine grain microstructures may also improve superplastic properties, which is particularly attractive in aluminum alloys for automotive applications. For this purpose, the effect of ECAE on the microstructural development and, correspondingly, superplastic tendencies in aluminum alloys was investigated.

Using ECAE to consolidate metallic powders may offer advantages not yet explored by conventional metal processing techniques, provided the processing temperatures are found to be lower than those required during hot isostatic pressure (HIP) consolidation. Subsequent heat treatment may also provide the benefits of homogeneous distribution of the second phase, resulting in precipitation

strengthening and thermal stability of grain boundaries. Powder consolidation by ECAE was, therefore, another focus of this investigation.

To summarize, the purpose of this investigation during the first year was to investigate the effect of ECAE processing on:

- Microstructural development, thermal stability, and corresponding mechanical properties of copper and its alloys (INEEL)
- Service life performance of resistance welding electrodes (INEEL)
- Microstructural development and superplastic tendencies in aluminum alloys for automotive applications (PNNL)
- Consolidation of copper with several different second phase powders (LANL).

2. ECAE DIE DESIGN, MATERIALS, PROCESSING, AND MICROSTRUCTURAL CHARACTERIZATION TOOLS

2.1 ECAE Design

2.1.1 ALCOA Die

In order to perform equal channel angular extrusions it was necessary to have a die and a load frame capable of exerting relatively large compression loads. To initiate this program as quickly as possible, an ECAE die was borrowed from ALCOA and installed on an Instron 225 kip (1,000 kN) hydraulic load frame located in the INEEL Research Center (IRC). This die consisted of a cylindrical barrel with a square hole in the center to accept a billet 1.25 inch square × 6 inches long. The billet was extruded around a 90° corner into a moving tray by compression loading with a ram. Further details of the die are considered proprietary by ALCOA.

The billet can be rotated between passes. Three rotation schemes, designated Route A, Route B, and Route C, were used. In the Route A, the billet was run through the die with no rotation between passes. Route B consisted of multiple passes with the billet rotated 90° between each pass, and Route C involved 180° rotation between passes. Figure 2 shows these routes schematically.

To become familiar with the die, Aluminum 1100 was ECAE-processed using Route A and up to six passes. No problems were encountered with the 1100 aluminum and therefore Copper Alloy 101 (commercially pure, oxygen-free copper) billets were prepared and processed through the die. Extruding copper required considerably higher loads than experienced with the aluminum. At first, limits were set on the load frame so when second pass loads were encountered that exceeded values formerly used by ALCOA, the loading was halted. Once the extrusion was stopped, extremely high loads (nearing the load frame's capacity) were unable to continue the extrusion and the die had to be disassembled to remove the sample. Varying the cross-head speed, route, and lubricant did make a difference on the loads required to extrude a sample. Figure 3 shows the effect on the lubricant used, which indicates that the Permatex Anti-seize gave the lowest loads on the first pass of copper billets.

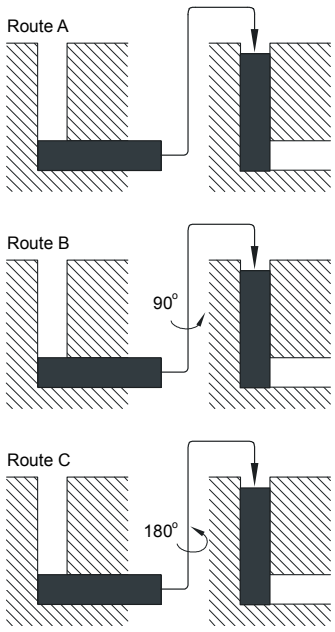

Figure 2. ECAE routes.

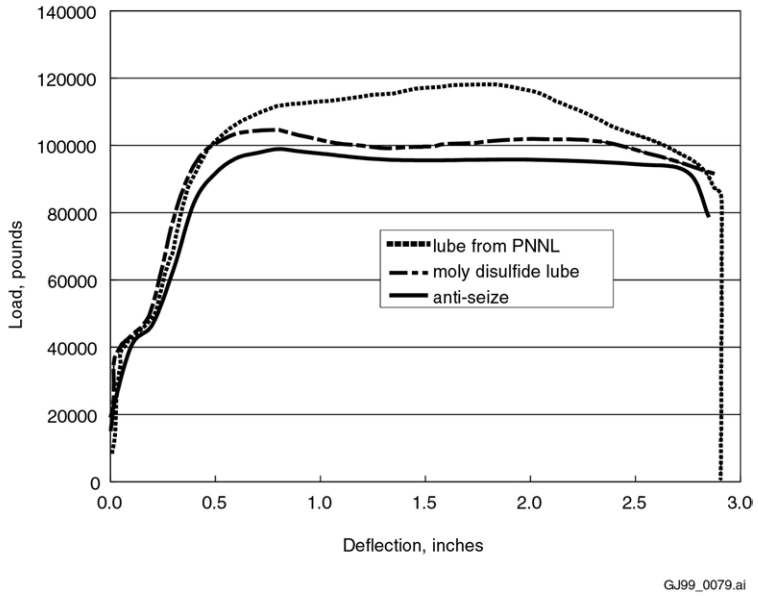

Figure 3. Effect of different lubricants.

Route B resulted in the highest extrusion loads and the billet had to be shortened from the six inches to four inches to stay within the 225 kip capacity of the load frame. Figure 4 shows the loads required for four passes using Route B with a four inch specimen. An interesting observation that was noted during the ECAE processing involved a 1 h, 200°C intermediate annealing of the specimen between the second and third pass. Even though the hardness was reduced markedly by the intermediate anneal, the load required to extrude the sample through the third pass was approximately the same as a sample without the anneal. The load did not appear to be affected by the anneal.

Varying the cross-head speed (strain rate) had a minimal effect on the extrusion loads as illustrated in Figure 5. The lowest cross-head speed used (10 mm/min) did result in a slightly lower load in the initial stages of extrusion but the loads for all rates blended together after this initial stage.

After the various operating parameters of the die were identified, eight billets of copper were ECAE-processed at room temperature using all routes and up to six passes. Aluminum alloy 5083 samples were also processed through the die, but at room temperature it was noted that large shear cracks were present after just one pass. The die was equipped with a heater and an attempt was made to process the 5083 alloy at 150°C, but again shear cracking, even though it was less, was observed. The die was then heated to 250°C and then two samples were successfully processed with four passes: one with the Route B and one with Route C.

2.1.2 New Die

It was noted from the ALCOA die that a significant portion of the load was due to friction between the specimen and the walls of the upper part of the die before extruding around the corner. When the load was first applied to the billet, the first thing it did was to barrel out and exert considerable pressure on the side walls of the die causing a high friction load. In an effort to minimize the friction loads, the new die designed by Vladimir Segal had side rails that moved with two sides of the billet as it was extruded around the 90° corner. Therefore, the sliding on these two sides was between two hardened and polished tool steel surfaces. Also the new die consisted of flat plates clamped together with bolts that eliminated machined internal corners which give rise to large stress risers. A schematic of the new die is shown in Figure 6. The size of the billet was scaled down for this die since the load machine for which it

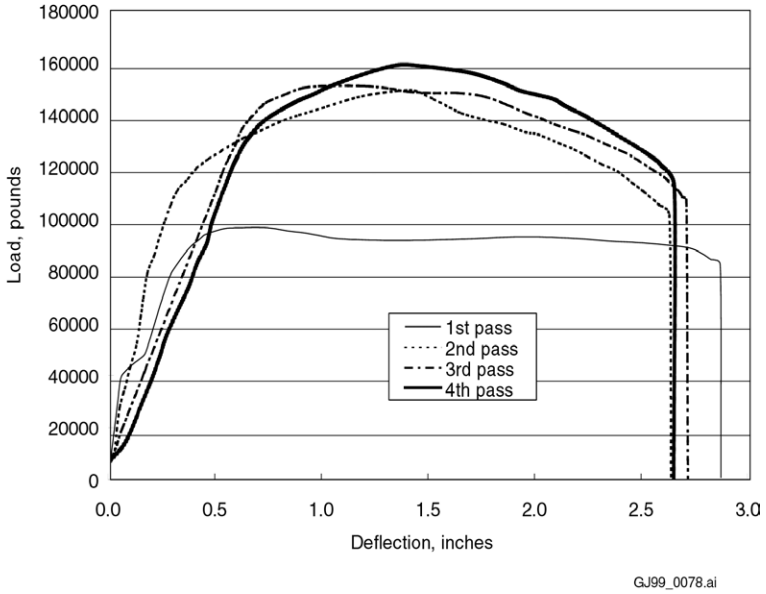

Figure 4. Loads required to extrude a four inch copper specimen using Route B.

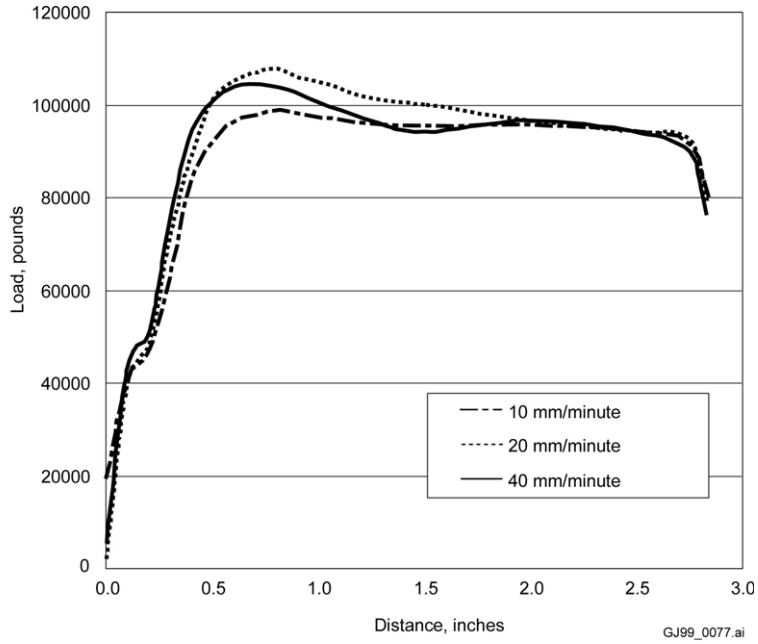

Figure 5. Effect of cross head speed on extrusion load.

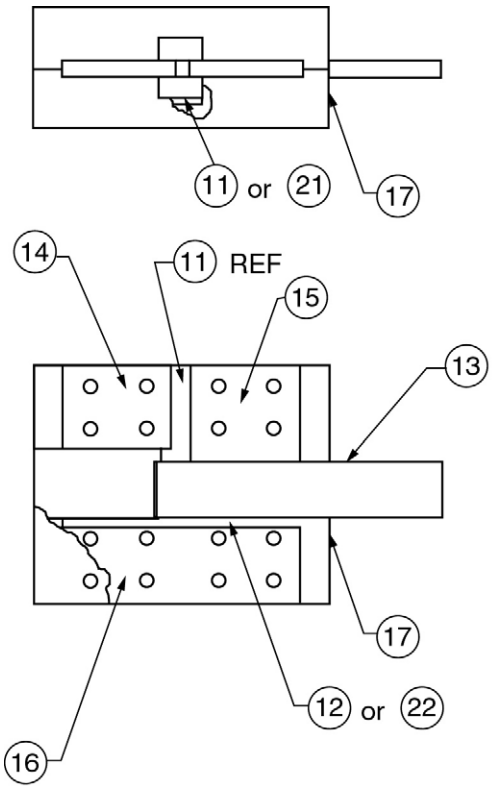

Item no.	Description
11 (21)	Vertical slide insert
12 (22)	Lower slide insert
13	Horizontal slide bar
14	Upper spacer, small
15	Upper spacer, large
16	Lower spacer
17	Side panels (2)
18	Punch
19	Vertical side rails (2)

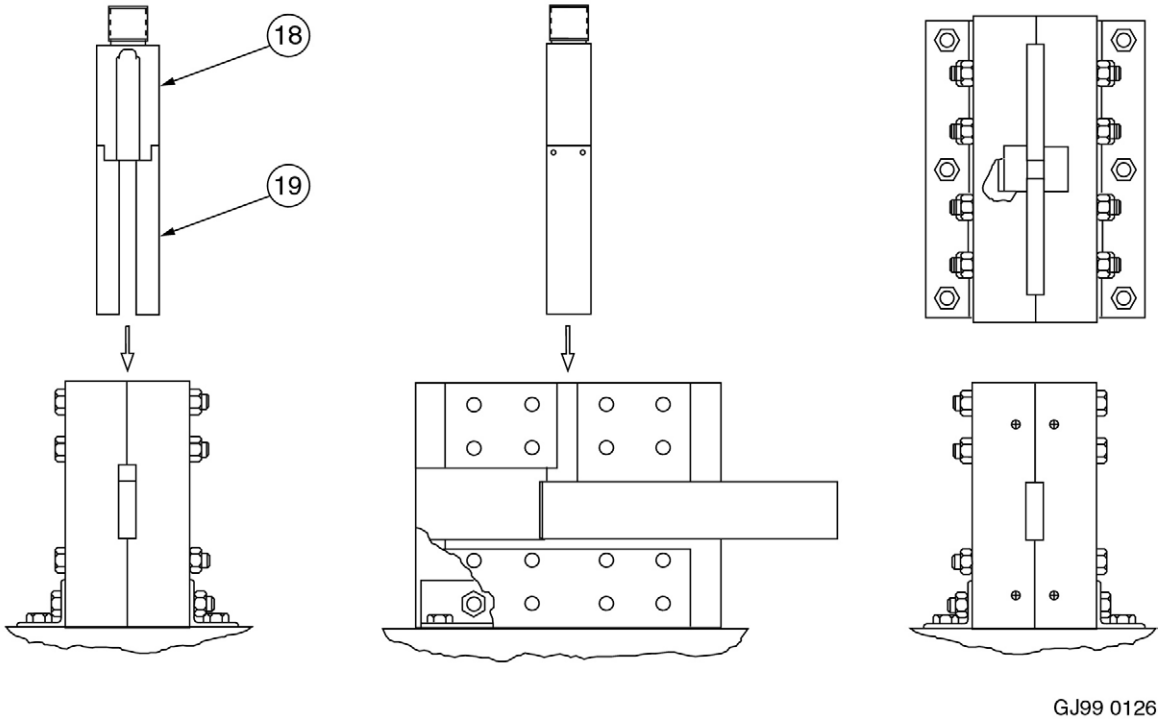

Figure 6. Schematic drawing of the new die.

was designed has a 100 kip load capacity. Therefore the new billet size is 0.88 inches square by 4.5 inches long.

Initial experience with the new die revealed that copper samples required near the full capacity of the load frame and that the extruded specimen exerted considerable friction forces on the side panels of the exit channel. When a relief of 0.02 inches was machined in the exit channel of the side panels, a significant load reduction was observed. Before the relief was incorporated, the load continued to increase as the length of the extruded specimen increased into the exit channel and the extruded specimen was nearly impossible to remove from the exit channel. After a relief was machined into the side panels, the specimen extraction was much easier. Three copper billets have been extruded through the die with four passes each using Route B. One brass (Cu-30wt%Zn) billet was extruded through one pass at room temperature, but the ear on one of the side rails failed on extraction of the punch/side-rail assembly. The side rails were redesigned to eliminate the sharp inner corner and the new design is currently in fabrication. Although there is some learning required in the operation and fine tuning of the new die, it appears to be working well. Currently a heating system is being designed for the die so that elevated temperature ECAE processing will be possible.

2.2 Materials, Specimen Designation, and Microstructural Characterization Tools

The following materials were considered in this part of the investigation.

- Oxygen-free copper, (.9999 purity)
- Dispersion-strengthened copper, designated by trade names Glidcop Al-15 and Al-60 (with 0.3 wt% and 1.1 wt% concentration of Al_2O_3 precipitates, correspondingly)
- Cu-0.7wt% Cr-0.1 wt%Zr alloy used for commercial resistance welding electrodes
- Pure aluminum and 5083 aluminum alloy.

The ECAE processing was performed at room temperature for pure copper and aluminum, and at 250°C for Al 5083. For a comparative study of the effect of ECAE vs. conventional cold rolling, several copper bars were prepared by cold rolling to 60 and 92% reduction in thickness and several bars were ECAE-processed with various routes and numbers of passes. These bars were machined into tensile specimens. Specimen designation is shown in Table 2.

The microstructural investigation used conventional optical microscopy, TEM, and Orientation Imaging Microscopy (OIM). OIM utilizes a scanning electron microscope in conjunction with high gain TV technology to analyze the flux of backscattered electrons and determine precise lattice orientation in small localized regions. This capability allowed information on grain boundary misorientation distribution and amount of special (high coincidence) boundaries in the microstructure to be obtained.

Table 2. Tensile specimen designations.

Annealing Temp., °C	Cold rolled		ECAE					
	60%	92%	1 pass	2 Passes/A	2 Passes/C	4 Passes/A	4 Passes/B	4 Passes/C
Room Temp.	Cu60-1	Cu92-1	Cu1A-1	Cu2A-1	Cu2C-1	Cu4A-1	Cu4B-1	Cu4C-1
200	Cu60-2	Cu92-2	Cu1A-2	Cu2A-2	Cu2C-2	Cu4A-2	Cu4B-2	Cu4C-2
300	Cu60-5	Cu92-5	Cu1A-5				Cu4B-5	
400	Cu60-3	Cu92-3	Cu1A-3	Cu2A-3	Cu2C-3	Cu4A-3	Cu4B-3	Cu4C-3
500	Cu60-7						Cu4B-6	
600	Cu60-4	Cu92-4	Cu1A-4	Cu2A-4	Cu2C-4	Cu4A-4	Cu4B-4	Cu4C-4

3. EXPERIMENTAL RESULTS

3.1 Comparative Study of ECAE Processing vs. Cold Rolling

3.1.1 Microstructural Characterization

Comparison of cold rolling vs. ECAE processing is given below in terms of microstructural characterization and mechanical properties data for the cold rolled and ECAE processed material. The cold rolling was conducted to 60% and 92% reduction in thickness, while the ECAE samples were extruded once via Route A (1A) or twice via Routes A (2A) or C (2C). The total imposed strain for 1A billets was 1.15, which compares closely with a total strain of 1.06 for the 60% cold rolled material. Billets 2A and 2C were subjected to 2.3 total strain, which compares to 2.63 total strain for the 92% cold rolled material. Subsequently, the billets were exposed to elevated temperature for 1 h. The temperatures and resulting grain size (as determined by OIM) are given in Table 3.

3.1.2 As-Processed Samples

TEM results of as-processed Cu60, Cu92, 1A, and 2C are shown in Figure 8. Visual analysis of microstructures does not reveal significant differences; all samples exhibit a lamellar structure consisting of elongated cells, though the cells in the 2C sample appear to be more equiaxed.

Misorientation distribution data (obtained by OIM) of the as-processed samples are shown in Figure 9. The amount of twin boundaries (misorientation angle of 60 degrees) retained during cold rolling to 92% and via the 2C path is small and comparable in magnitude: 1.9% for 2C and 1.7% and 1.8% for Cu92Z and Cu92X correspondingly.

Table 3. Annealing temperature and resulting grain size.

Specimen[a]	Temperature, °C	Grain Size, μm	Twin Boundary Fraction
Cu60-1	RT	Not defined[b]	0.02
Cu60-5	300	23.9	0.46
Cu60-3	400	21.5	0.49
Cu60-7	500	25.5	0.49
Cu60-4	600	27.1	0.4
Cu92-1X	RT	Not defined[b]	0.021
Cu92-1Z	RT	Not defined[b]	0.017
Cu92-2X	200	3.52	0.2
Cu92-2Z	200	5.41	0.19
Cu1A-3	400	Not defined[b]	0.32
Cu2C-aex,X	RT	Not defined[b]	0.019
Cu2C-aex,Y	RT	Not defined[b]	0.039
Cu2C-200,X	200	5.58	0.52

a. X, Y, and Z designate the face of the extrusion billet, as shown in Figure 7.

b. The as-deformed microstructure consists of fine grains and high density of dislocation cells with low angle grain boundaries. Definition of grain size by OIM in this case is difficult, since the measured grain size in such microstructures is very sensitive to the definition of the grain boundary misorientation angle at which dislocation cells are considered grains.

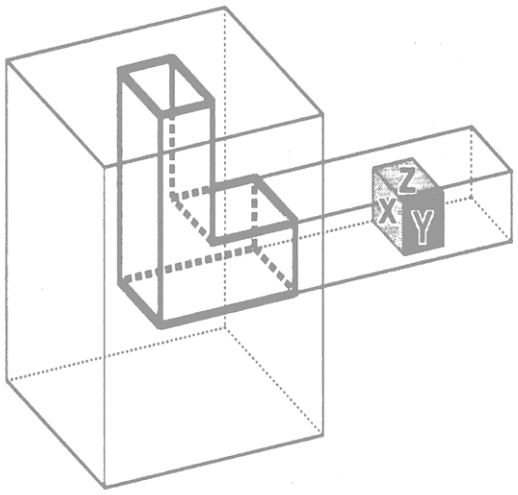

Figure 7. Billet orientations on last pass.

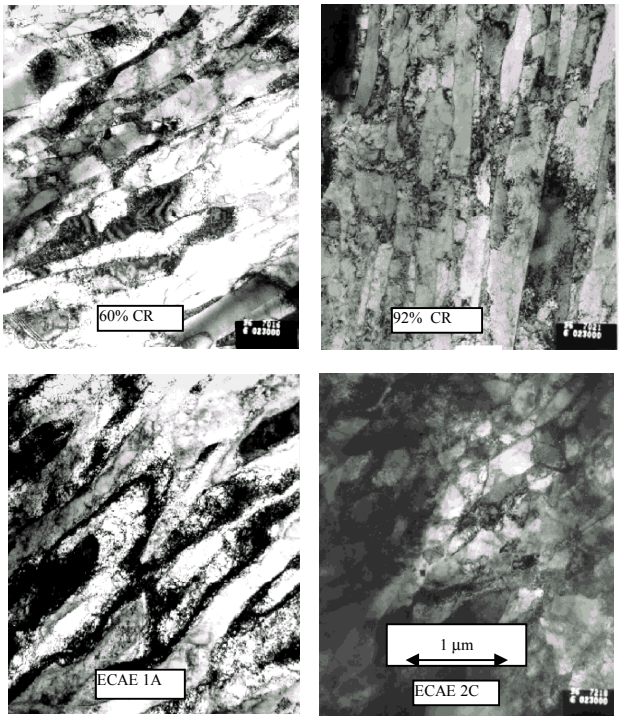

Figure 8. TEM micrographs showing the effect cold rolling vs. ECAE processing on microstructure.

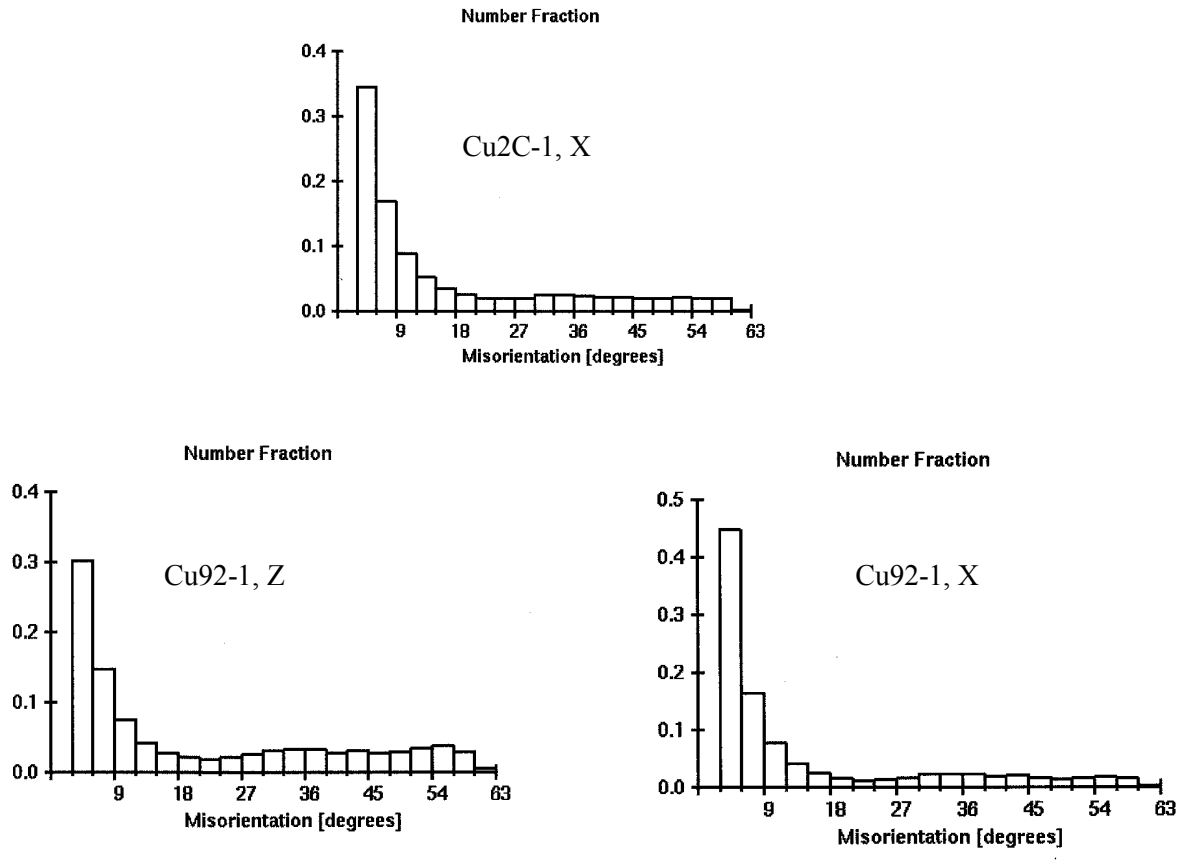

Figure 9. Bar graphs showing number fraction and misorientation angles between grains.

3.1.3 Annealed Samples

Misorientation distribution data of the annealed material are shown in Figures 10 and 11. The amount of special boundaries detected on faces X and Z of Cu92-2 are approximately the same, and much lower than that in Cu2C. In addition, more low angle grain boundaries are detected on Z than on X face of the Cu92 sample.

OIM analysis results of the annealed samples are shown in Figures 12 and 13. The grains in Cu92-2X appear to have elongated in the rolling direction, whereas the grains in the Cu92-2Z are more equiaxed. Both samples show a large variation in grain size, indicating possible regions of recrystallized and unrecrystallized microstructures, while the grain size distribution of the Cu2C-2 appears to be more homogeneous. The difference in the presence of the unrecrystallized area may account for different volume fraction of twin boundaries present in the annealed samples.

3.1.4 Mechanical Test Data

The mechanical properties of the cold rolled and ECAE-processed samples appear to be very similar, as evidenced by the yield and ultimate strength and maximum elongation values. The summary of these data is shown in Table 4.

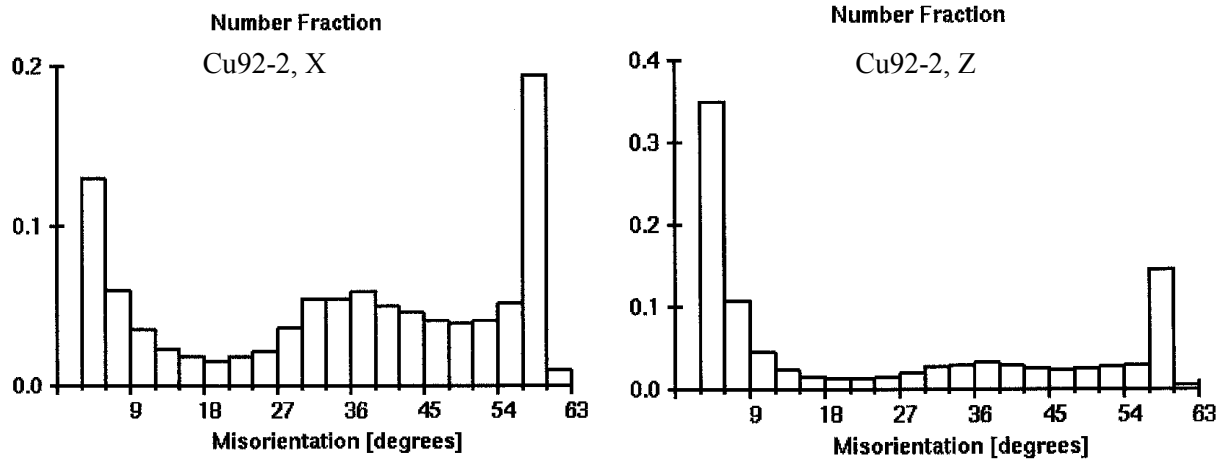

Figure 10. Misorientation data of Sample Cu92-2 (X & Y faces) after annealing 1 h at 200°C.

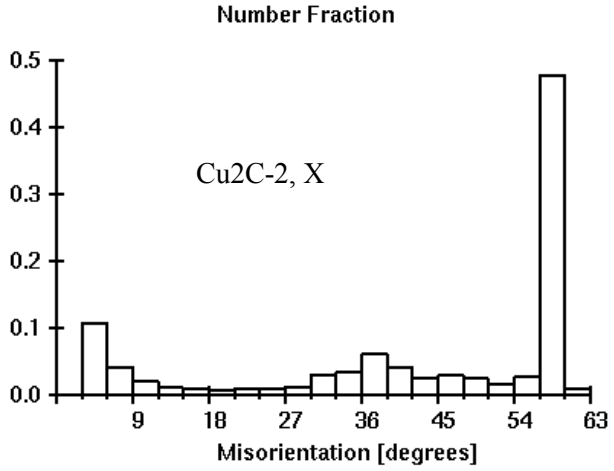

Figure 11. Misorientation distribution data of Cu2C-2 after 1 h 200°C anneal.

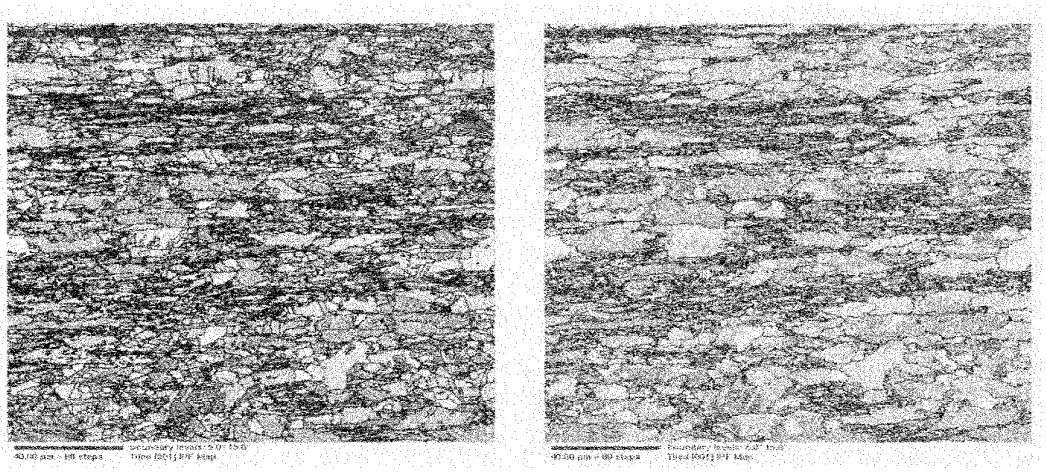

(a) Cu92-2, X

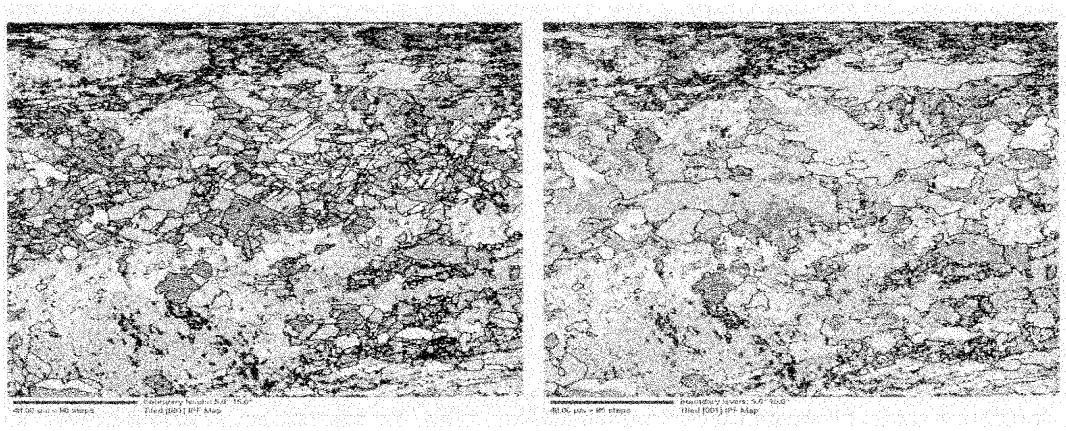

(b) Cu92-2, Z

Figure 12. OIM micrographs of Cu92-2 annealed 1 h at 200°C.

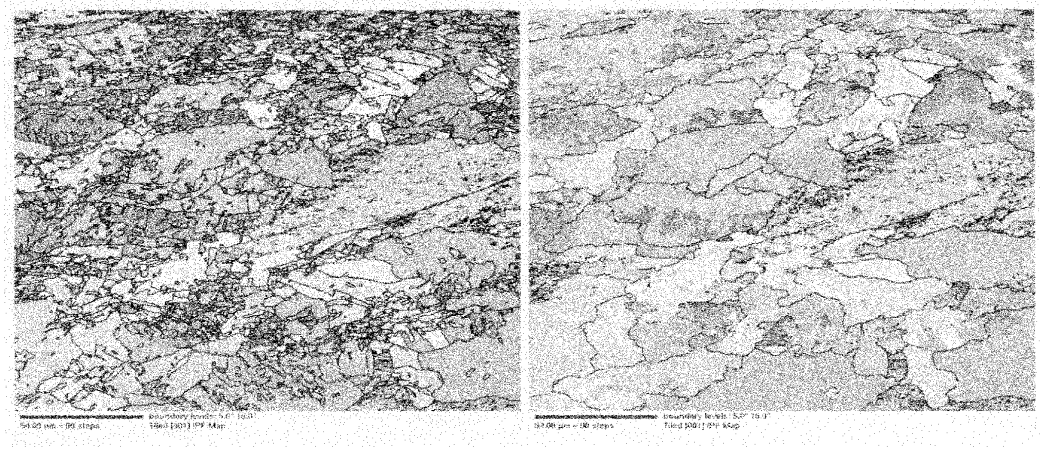

Figure 13. OIM micrographs of Cu2C-2X.

Table 4. Room temperature mechanical property data of rolled and ECAE processed copper.

Specimen	Annealing Temperature, °C	Yield Stress, ksi	Ultimate Stress, ksi	Total Elongation, %
Cu60-1	RT	47.5	48.1	15.6
Cu60-2	200	45.6	46.4	16.5
Cu60-3	400	6.3	31	63.6
Cu60-4	600	5.4	29	63
Cu60-5	300	6.2	31.4	59.7
Cu60-6	500	5.5	30.8	59.3
Cu92-1	RT	53.8	55.1	3.05
Cu92-2	200	15.6	38.1	35.5
Cu92-3	400	5.9	31.6	58.1
Cu92-4	600	6.4	31.5	56.3
Cu92-5	300	9.2	31.3	35.5
Cu1A-1	RT	48.5	49.7	14.7
Cu1A-2	200	45.6	47.3	18.9
Cu1A-3	400	6.3	31.1	60
Cu1A-4	600	5.4	29.7	62.5
Cu1A-5	300	5.4	31.5	59.6
Cu2A-1	RT	53.5	54.3	14.5
Cu2A-2	200	18.3	37.9	39.9
Cu2A-3	400	7.4	31.8	59.8
Cu2A-4	600	5.5	29.2	64.6
Cu2C-1	RT	54.1	56.2	13.2
Cu2C-2	200	12	35.1	43.8
Cu2C-3	400	5.8	31.4	60.4

The plots of the yield strength as a function of the annealing temperature are shown in Figures 14 and 15. It can be seen that the Cu60 and CuA1 show a drop in yield strength in the temperature range between 200 and 300°C, indicating a region where recrystallization took place. The recrystallization temperature of the samples (Cu92, CuA2, and CuC2) that have undergone larger deformation is lower, probably around 100°C.

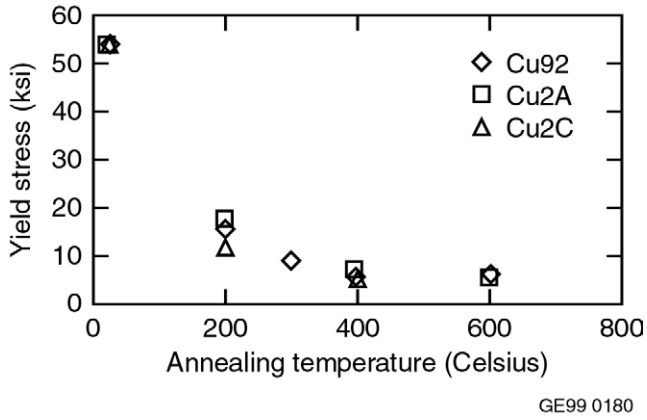

Figure 14. Effect of annealing temperature on yield stress for Cu92, CuA2, and CuC2 samples.

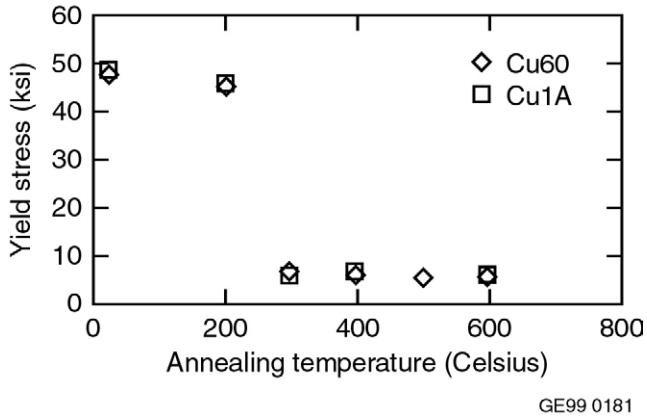

Figure 15. Effect of annealing temperature on yield stress for Cu60 and Cu1A samples.

3.1.5 Conclusions

The following conclusions can be made based on the obtained microstructural characterization and mechanical testing data.

The 92% and ECAE–processed Cu2C samples exhibit similar microstructural evolution. The samples contain a very limited amount of twin boundaries. The dislocation cell formation is even more pronounced in this case than that in Cu60 and 1A samples.

With the exception of the cold-rolled samples annealed at 200°C, heat treating of the deformed samples results in microstructures with very high fraction of twin boundaries. The cold-rolled samples, when annealed at 200°C, show a presence of unrecrystallized regions, which is a probable cause of a comparatively low fraction of annealed twin boundaries in those samples.

Mechanical properties of the cold rolled and ECAE processed samples are similar. The ECAE processing does not appear to produce materials which, when compared with materials cold-rolled to similar strain magnitudes, possess unique mechanical behavior with respect to such properties as yield and ultimate strength and total elongation.

3.2 Effect of ECAE Processing on Microstructure and Mechanical Properties

It is conceivable that differences in microstructure could arise in samples processed by the different routes due to the variation of the deformation vector. This set of experiments was, therefore, performed to assess the effect of the processing route on the microstructure and properties of pure copper. Comparisons were made after a total of 4 passes for a total strain of ~4. Annealing behavior was also investigated for samples subjected to equal total strain but differing processing routes. One hour anneals were carried out at 200, 400, and 600^{o}C. Samples were heated at 10^{o}C/minute to the annealing temperature. Samples were characterized with optical and transmission electron microscopies as well as OIM and mechanical testing.

3.2.1 Microstructural Characterization

3.2.1.1 As-processed samples. Transmission electron microscopy was used to evaluate the as-processed microstructure. The microstructures arising from the different processing routes are shown in Figure 16. Subtle differences in microstructure are observed in the samples processed by the three different routes. The sample processed by Route A, Figure 16a, exhibits an elongated cell structure. Samples processed by Route B, Figure 16b, consisted of a cell structure that was more equiaxed than samples processed by Route A and C. (Also, very little difference between the x- and y-faces for each processing route is observed. The z-face was expected to closely resemble the y-face and was not investigated.) The cell size and aspect ratio are recorded in Table 5. These results are not surprising since the deformation was always imposed in the same direction in Route A while the sample processed by Route B experienced equal deformation in four different directions. Route C can be envisioned as a bending/unbending operation and is expected to produce a directional microstructure similar to that produced by Route A.

Figure 17 shows the results of the OIM scans, with boundaries of greater than 10^{o} misorientation outlined in black, on material processed by Routes A and C. (The method used to mount the Route B samples caused them to recrystallize and their microstructure was no longer representative of as-extruded material.) Route C is observed to produce a finer and more uniform microstructure. The grain size for each processing route as obtained from OIM measurements is also recorded in Table 5. These values generally agree with those determined from TEM. Figures 18a and 18b show the distribution in grain sizes obtained by OIM in materials processed four times by Routes A and C, respectively. The distributions for Routes A and C do show significant differences with the Route A producing a flatter

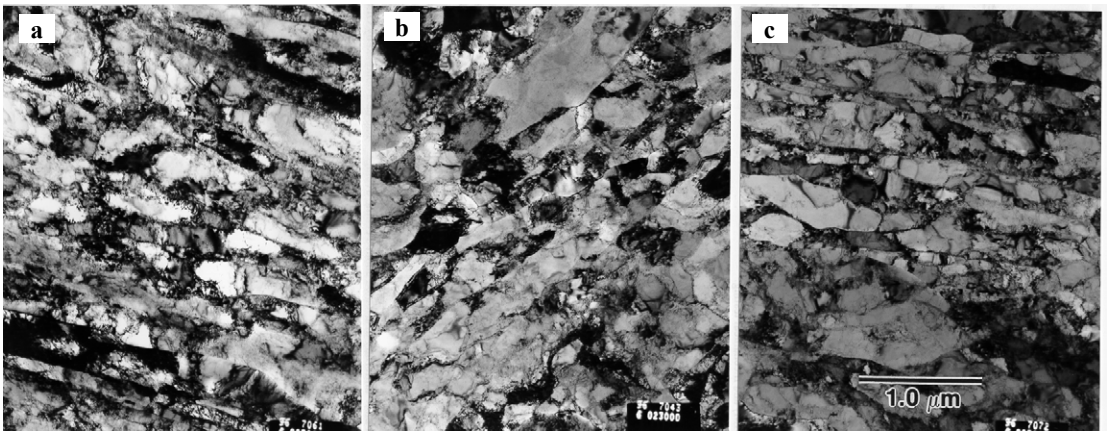

Figure 16. Microstructure of copper after four passes by a) Route A, b) Route B and c) Route C.

Table 5. Grain size of ECAE samples after four passes.

Sample	Grain Size[a] TEM, µm	Aspect Ratio (TEM)	Grain Size[a] OIM, µm
Cu4A	0.28	4	0.49–0.23
Cu4B	0.20	1.5	NA
Cu4C	0.22	2.5	0.34–0.15

a. Assumes a round grain, $d=2*(Area/4*\pi)^{1/2}$

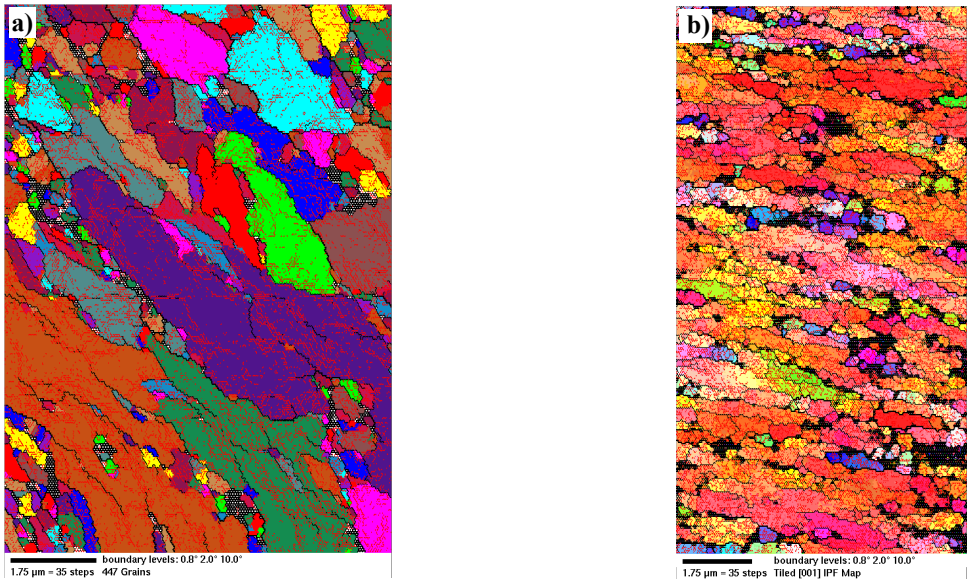

Figure 17. Microstructures recreated from OIM data for a) Route A, four passes and b) Route C, four passes. Grains are based on the crystallographic misorientation between adjoining analysis points.

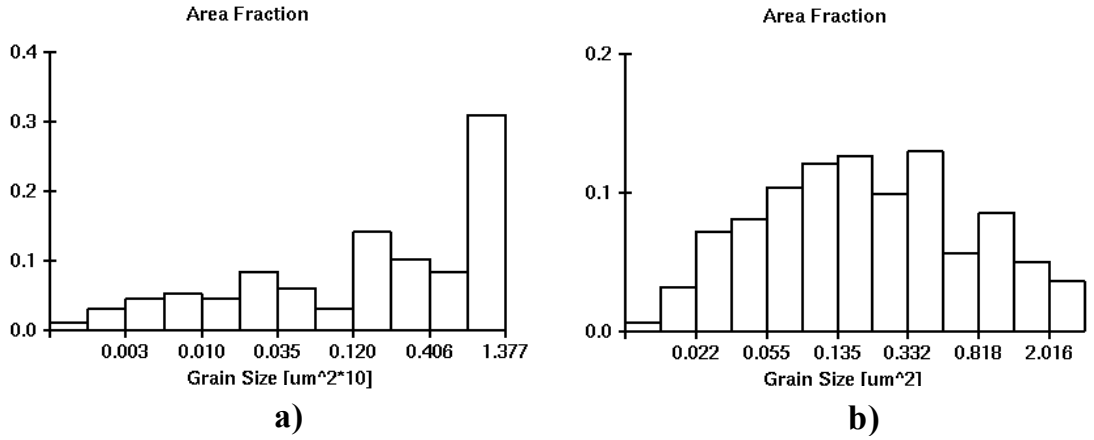

Figure 18. Grain size distribution for the x-faces of samples a) Route A, four passes and b) Route C, four passes.

distribution than Route C that is more uniformly distributed about a central average. The data obtained by OIM was also used to show the distribution in misorientations in the as-extruded materials. The misorientation distribution plots in Figure 19 indicate most of the grain boundaries are of very low angle indicating a deformation cell structure.

3.2.1.2 Annealed Samples. Recrystallization was found to occur at temperatures below 200°C. Optical microscopy, OIM, and TEM all revealed that recrystallization had produced a very high twin density in the annealed ECAE samples as shown in Figures 20 and 21. The misorientation distribution

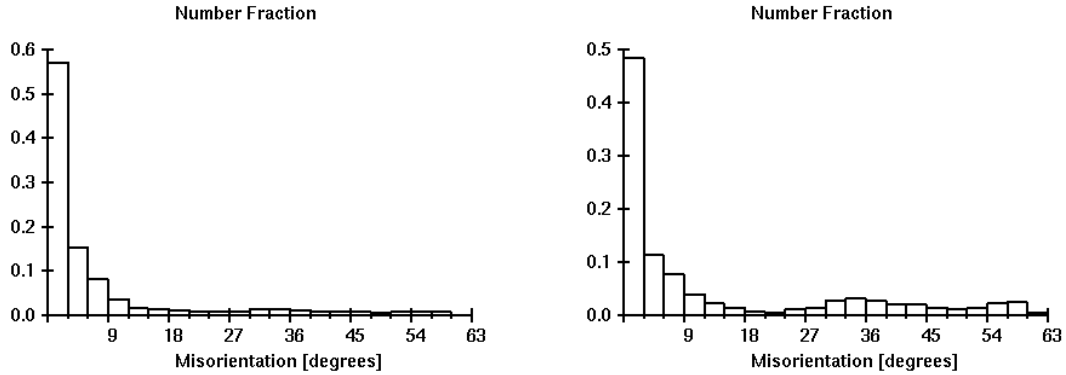

Figure 19. Distribution of grain boundary misorientations for a) Route A, four passes and b) Route C, four passes.

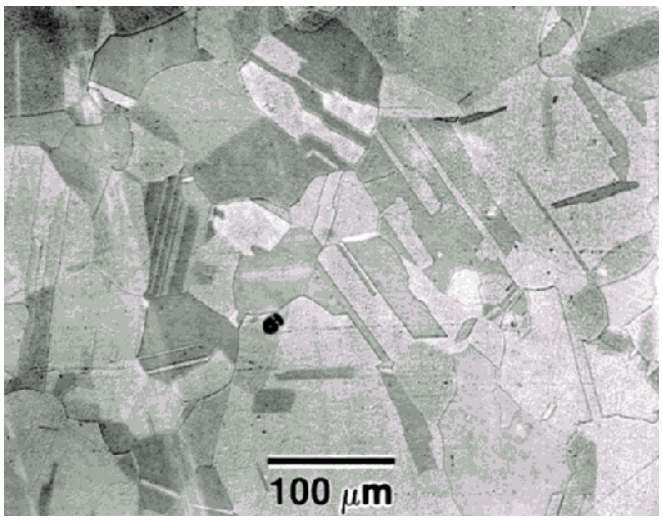

Figure 20. Optical photomicrograph showing a high twin density in Sample Cu4B, annealed at 600°C for 1 h.

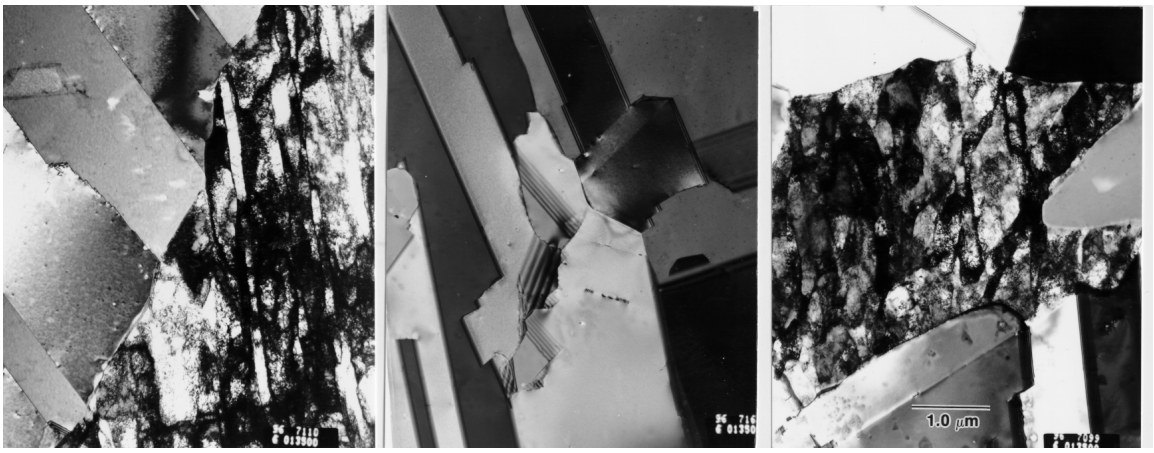

Figure 21. Bright field TEM micrographs showing a high density of twins. Also, unrecrystallized material is observed in the Cu4A and Cu4C, 200°C annealed samples but lacking in the Cu4B, 200°C annealed sample.

function was calculated from the OIM data with a representative plot shown in Figure 22. Immediately evident in these plots is the large fraction of Σ3 grain boundaries, i.e. twins. The annealing temperature appears to have a weak, though significant, effect on the number fraction of twins in the final microstructure as shown in Figure 23.

As shown in Figure 21, TEM revealed residual unrecrystallized areas in the 4A and 4C samples but very little in the 4B samples, after a 200°C anneal. It is possible that this is simply due to the small sample sizes explored in the TEM or that samples processed by Route B contained more stored energy that produced a higher driving force for recrystallization. Recrystallized grain size as a function of annealing temperature is plotted in Figure 24. This plot indicates the recrystallized grain size is not a strong function of ECAE processing path at equivalent total plastic strain. The OIM

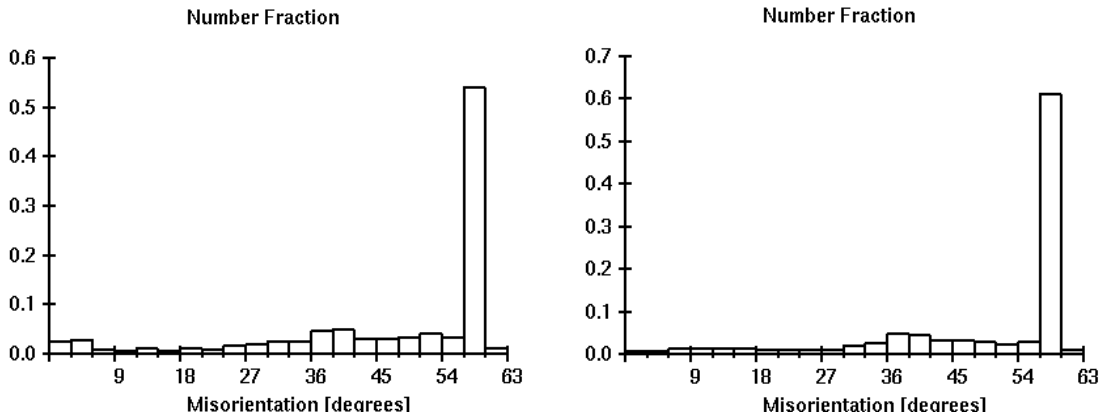

a) Sample 4A, X–Face, 400°C b) Sample 4C, X–Face, 400°C

Figure 22. The misorientation distribution function for Routes A and C, four passes, annealed at 400°C for 1 h. Twin boundaries comprise a major fraction of the grain boundaries present. This observation was typical for all annealed samples.

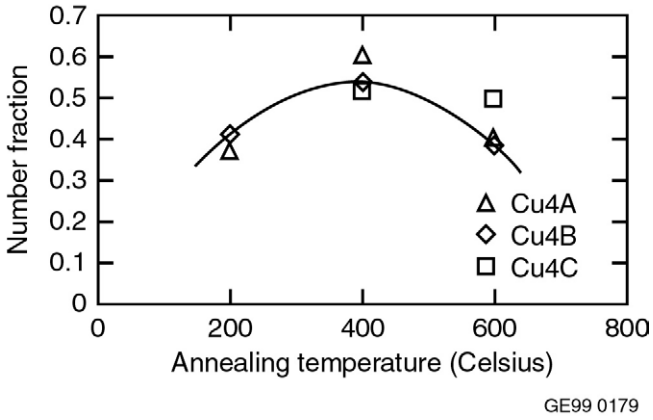

Figure 23. Plot shows the fraction of twins as a function of annealing temperature.

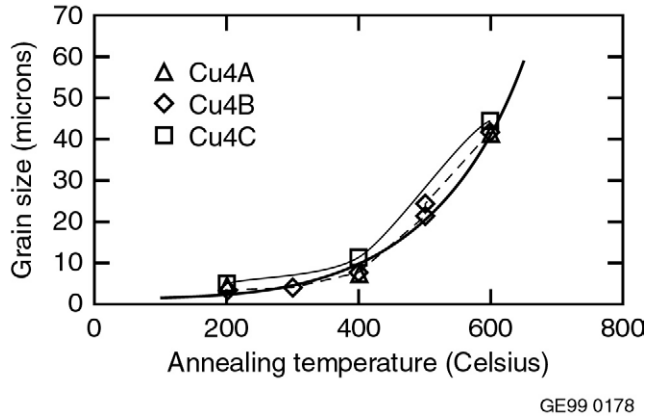

Figure 24. The three different ECAE processing routes produce only minor differences in grain size after recrystallization. Twin boundaries have been included in the grain size measurements.

data was also used to assess the presence of texture elements in the recrystallized samples. Generally, only weak textures were found. Figure 25 shows a typical intensity pole figure plot were it is seen that the texture elements have an occurrence of ~2.7 times random. Most pole figures showed elements on the order of 2–3 times random with some reaching as high as ~8 times random which is not considered strong texturing. The dominant texture elements were different for samples annealed at different temperatures as well as processed by the different ECAE routes.

3.2.2 Mechanical Properties

There was surprisingly little difference in the mechanical properties of the material processed four times by the different ECAE routes. Generally, the true stress-true strain plots appeared very much like that shown in Figure 26 with the yield stress, ultimate tensile stress and elongation being dependent on annealing history only and not on processing path. The data for the differently processed sample are shown graphically in Figure 27.

3.2.3 Conclusions

The following observations were made following analysis of the data:

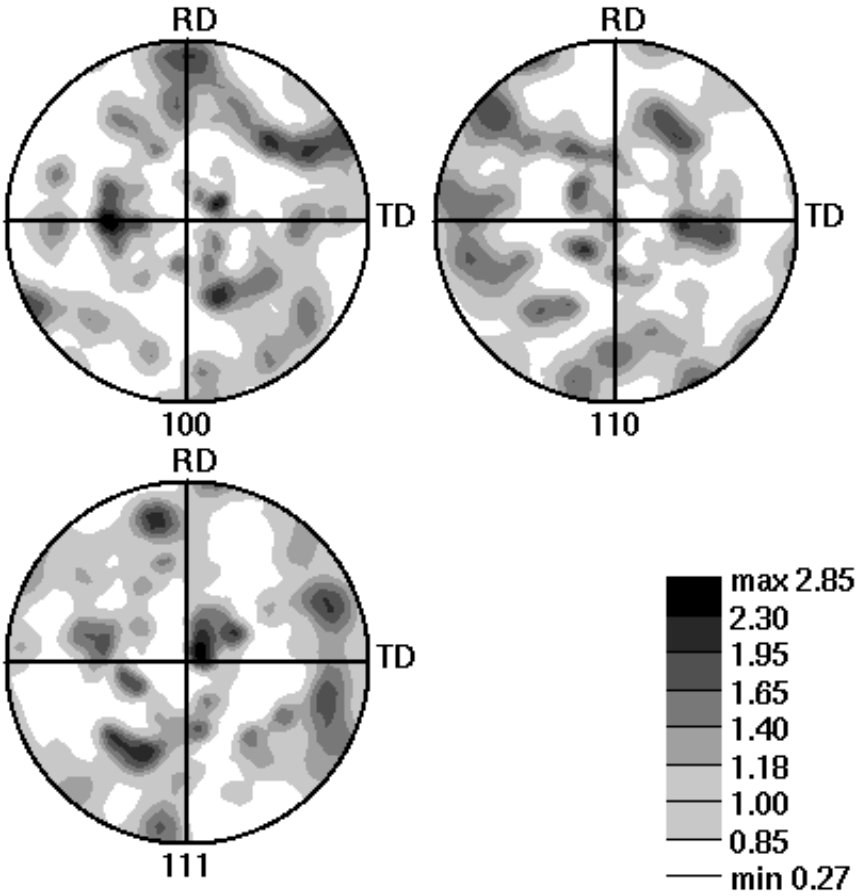

Figure 25. Intensity pole figure plot produced from OIM data showing the extent of texturing for Route A, four passes, annealed at 400°C, x-face. The dominant texture elements of the other samples were generally around 2–3 times random although different texturing elements were present.

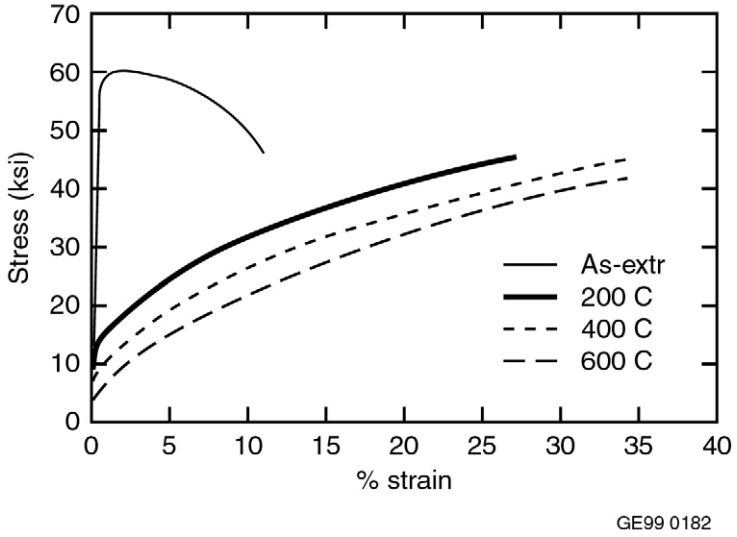

Figure 26. Plot of true stress versus true strain for Route C, four passes.

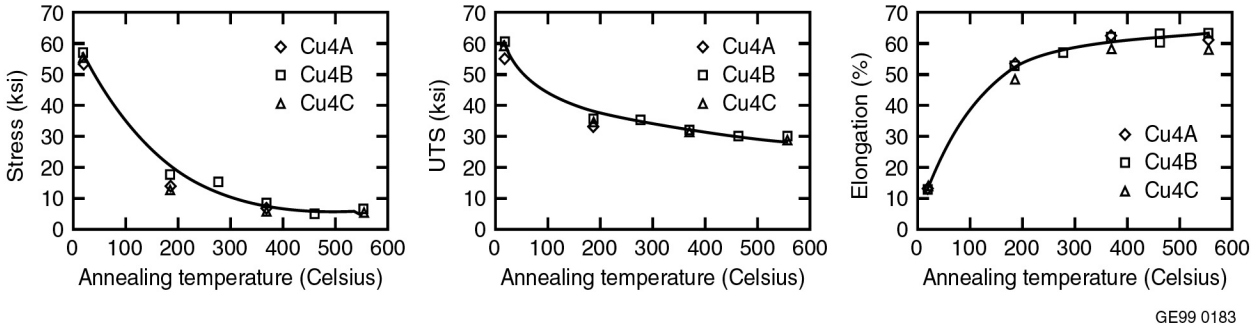

Figure 27. Annealing effect on the yield strength, ultimate strength, and elongation of the four pass copper samples with Routes A, B, and C.

- ECAE produces a submicron grain size in copper after four passes
- Route B appears to produce the most equiaxed microstructure
- Recrystallization takes place at temperatures below 200°C after four passes, regardless of processing route
- Recrystallization produces a high density of twins in ECAE material
- ECAE does not produce strong textures, even after recrystallization
- Tensile properties are not greatly affected by ECAE processing route after four passes
- After four passes, the microstructure, cell size, recrystallized grain size and tensile properties are not strongly dependent on processing route.

4. FLOW STRESS BEHAVIOR OF ANNEALED OFHC COPPER AFTER LARGE DEFORMATIONS

An opportunity to unravel the microstructure-flow stress association for the true stress-true strain tensile behavior of polycrystalline, oxygen-free high-conductivity (OFHC) copper was realized from material processed by cold rolling and ECAE. This study was performed on OFHC copper specimens prepared from material cold-rolled (60% reduction in thickness and a corresponding true strain of ~116%) and cold ECAE (Route B configuration with four passes designated as 4B that produced a true strain, mostly shear, of ~400%). These two cold forming methods are, in principle, quite diverse and provide an opportunity to assess their influence on the microstructure and tensile properties after annealing. The annealing treatments given to tensile specimens involved exposure for 1 h at temperatures from 200 to 600°C. This series produced a range in grain sizes. Supporting microstructural information for the flow stress behavior was obtained from optical, transmission electron, and orientation imaging microscopy.

4.1 Experimental Results

Representative true stress-true strain tensile curves from room temperature tests are shown in Figure 28 for the ECAE Cu4B and Cu60 specimens. The curves indicate that the flow stress decreases with increasing heat treat temperature, suggesting a grain size influence.

Grain sizes were obtained on transverse sections from the grip region of the tensile specimens. Measurements involved the linear intercept method performed on micrographs from optical as well as orientation imaging microscopy (OIM). Grain resolution comes from chemical etching for the former and grain orientation for the latter. A comparison of the image quality for the microstructure is shown in Figure 29 for the Cu4B and Cu60 specimens annealed at 400°C. It is apparent that the grain resolution is comparable. The average boundary intercept values and corresponding grain sizes for the Cu4B and Cu60 series of specimens are shown in Table 6. It should be noted that the twin boundaries were included in the intercept measurements. Results show that the grain sizes obtained from both optical and orientation microscopy are nearly equivalent.

The OIM analysis of the specimens provided additional information in association with grain orientation effects. The measurements produced coincident site lattice (CSL), Taylor factor, and Schmid factor orientation values. These results are shown in Table 7. The CSL values are for $\Sigma 3^n$ which are closely associated with twin orientations. The results in Table 7 show comparable orientation features for the copper whether processed by cold rolling or ECAE. There does not appear to be an influence of grain size/annealing temperature on the Taylor and the Schmid factors. However, there may be a modest dependency of the $\Sigma 3^n$ CSL fraction with grain size/annealing temperature, at least for the Cu4B series.

4.2 Analysis of Results

The true stress-true strain curves shown in Figure 28 suggest a parabolic relationship. The flow (true) stress is plotted against the square root of total true strain, $(\varepsilon_t)^{1/2}$, in Figure 30 with a) Cu4B and b) Cu60 series. The flow stress behavior for the copper series appears to show three stages that we will reference as I, II, and III. Stage I falls into the microyield/microdeformation category,[3-8] and is primarily associated with total true strains ≤ 0.004. This region appears to be grain size dependent. Stage II has a limited strain (total) range of ~ 0.004 to 0.010 and appears to be independent of grain size since the slopes of the flow stress curves are nearly constant for the nine copper specimens examined in this study. Stage III for true strains > 0.02 shows a constant slope of 498 (+18-28 range) MPa for the combined Cu4B and Cu60 series; therefore, also independent of grain size.

Table 6. Boundary intercept and grain sizes of Cu4B and Cu60 copper specimens after annealing.

Specimen	Annealing Temp.,°C	Average Intercept, mm		Average Grain Size, mm	
		OIM	Optical	OIM	Optical
Cu4B	200	0.00215	0.00296	0.0023	0.0033
	300	0.0037	0.0040	0.0041	0.0045
	400	0.0083	0.0071	0.0093	0.008
	500	0.0201	0.0171	0.022	0.019
	600	0.0374	0.0440	0.042	0.052
Cu60	300	0.0278	0.0249	0.031	0.028
	400	0.0346	0.0255	0.039	0.029
	500	0.0367	0.0324	0.041	0.037
	600	0.0383	0.0381	0.043	0.043

Table 7. Orientation measurements on annealed Cu4B and Cu60 copper specimens.

	Annealing Temperature,°C	Fraction CSL-$\Sigma 3^n$	Taylor Factor	Schmid Factor[a]
Cu4B	200	0.65	3.01	0.46
	300	0.62	3.07	0.45
	400	0.52	3.09	0.45
	500	0.49	3.08	0.46
	600	0.51	3.07	0.45
Cu60	300	0.56	3.07	0.44
	400	0.55	3.11	0.44
	500	0.55	3.09	0.44
	600	0.45	3.03	0.45

a. maximum for favorable slip orientation is 0.50.

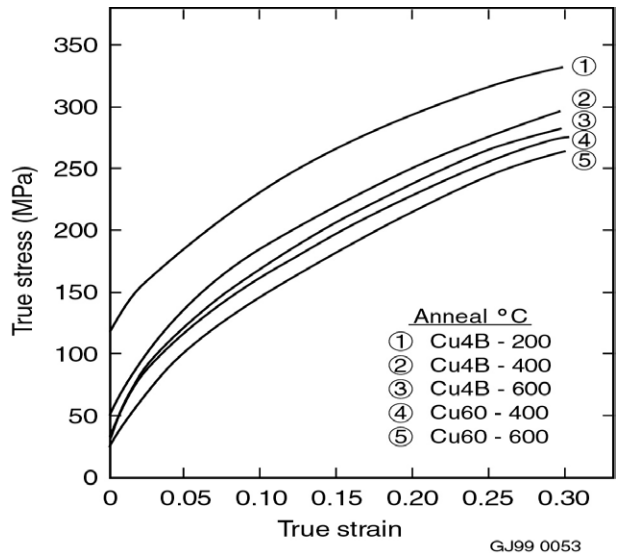

Figure 28. Influence of annealing temperature on the true stress-true strain tensile curves for cold rolled and cold ECAE processed copper.

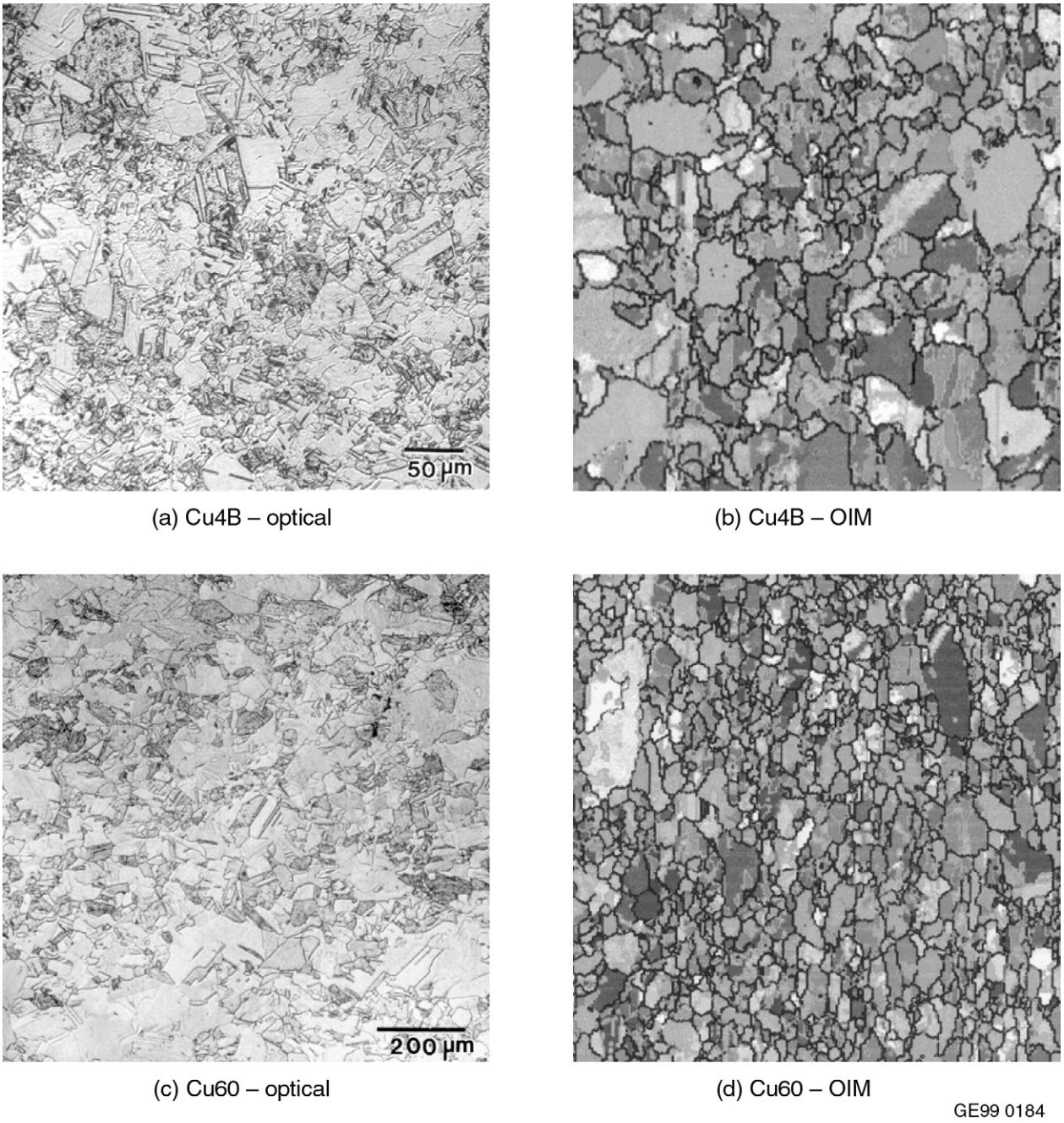

Figure 29. Grain morphology comparisons from optical and orientation imaging microscopy for copper of the annealing at 400°C. a) Cu4B optical, b) Cu4B OIM, c) Cu60 optical, and d) Cu60 OIM.

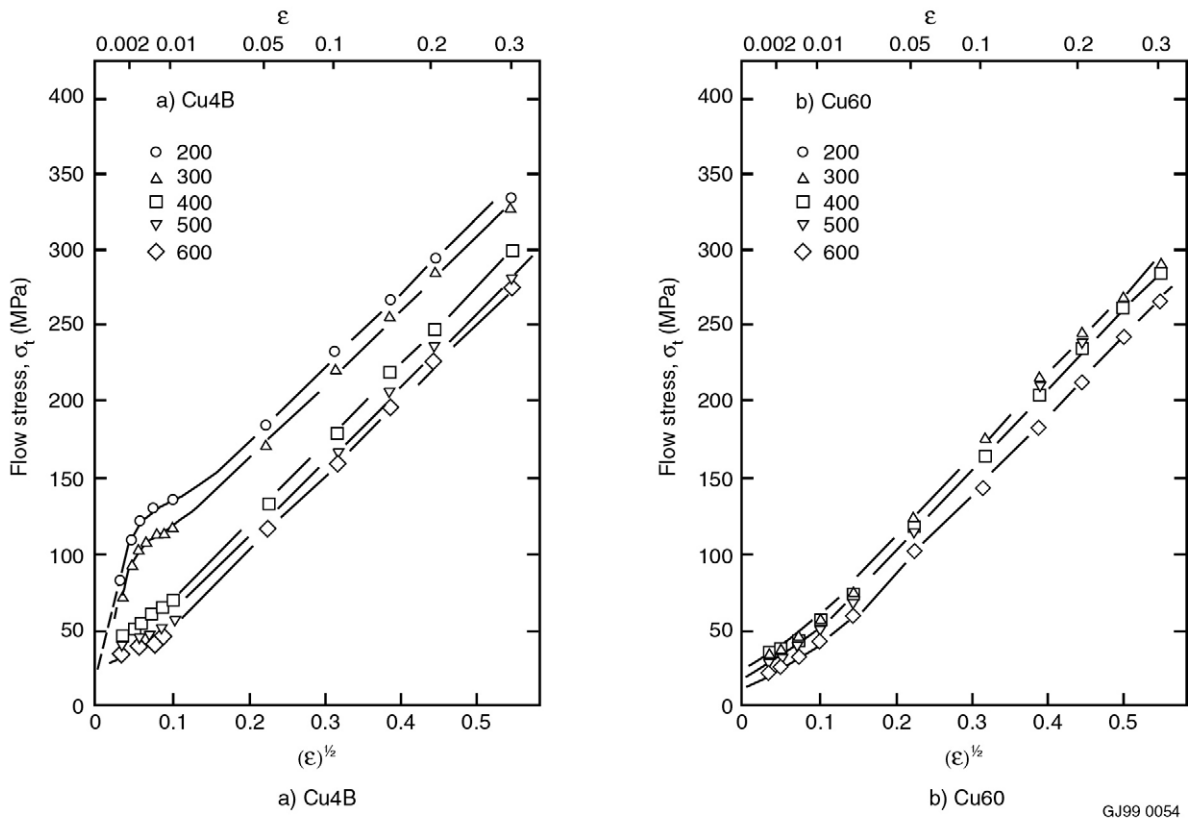

Figure 30. Flow stress dependence on the square root of true strain after 1 h annealing treatments.

The behavior associated with regions I and II is more apparent in Figure 31, where the flow stress is plotted against the square root of plastic strain, i.e., $\varepsilon_p = \varepsilon_t - \varepsilon_e$ where ε_p = plastic strain, ε_t = total strain, and ε_e is the elastic strain. The total true strain range for this plot is to 0.007. The specimens associated with the very small grain sizes (i.e., 200 and 300°C anneals) show evidence of a monotonic increase in flow stress and a nonlinear association with the square root of plastic strain up to ~ 0.002 plastic strain. At strains > 0.002, the designated Stage II has been initiated. Below plastic strains of .002 ($\sqrt{\varepsilon_p} = 0.045$), other investigators have shown nonlinear stress-strain behavior.[3,6,8] The average slope of the Stage II region is 286 (+60-45 range) MPa, and appears to be independent of grain size. The intercepts associated with Stage II has an apparent grain size dependence as shown in Figure 32 where σ_i is plotted against the reciprocal grain diameter.

4.3 Discussion of Results

The strain hardening behavior for polycrystalline copper appears to have two linear stages with respect to the square root of plastic strain. The flow stress behavior shows evidence that there are two transition strain regions with one preceding Stage II which we are designating here as Stage I. The other transition lies between Stage II and Stage III. For the polycrystalline copper examined in this study, it should be recalled that Stage III begins after strains > 0.02 have been obtained.

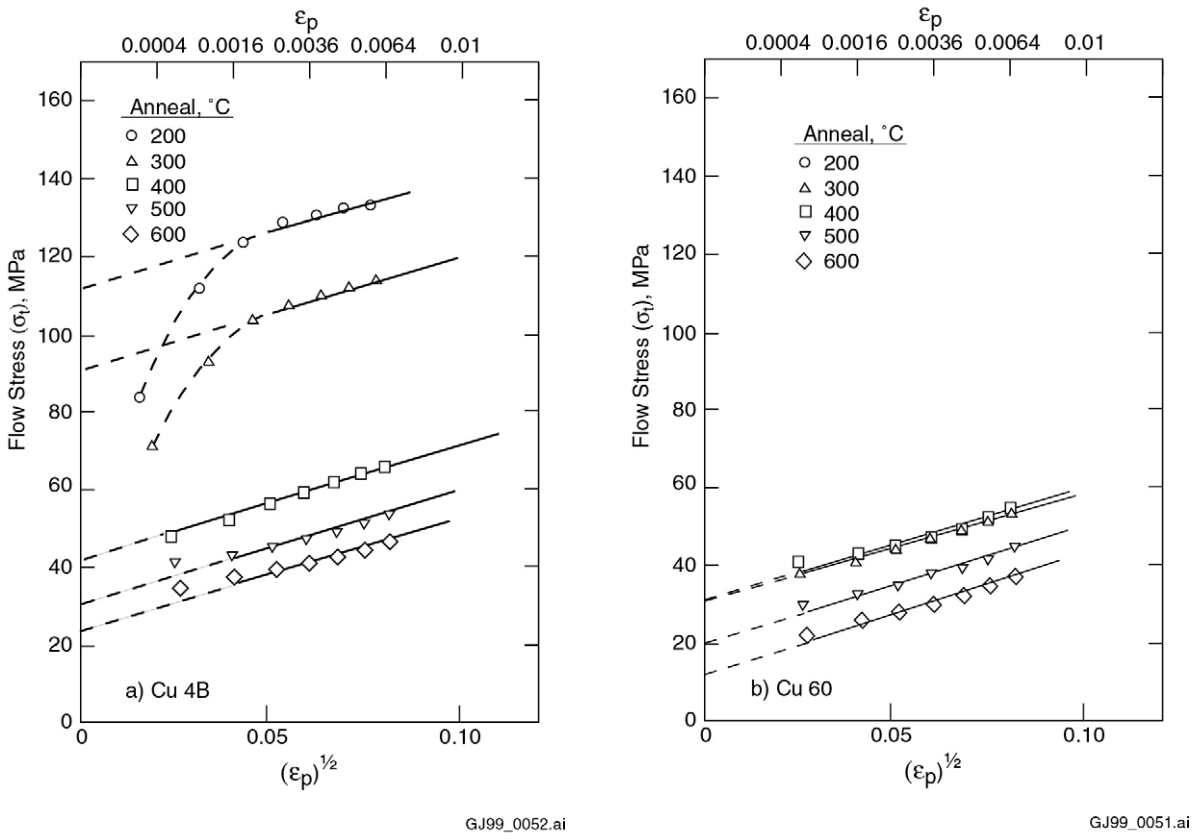

a) Cu4B b) Cu60

Figure 31. Flow stress dependence on the square root of true plastic strain in the low strain region after 1 h annealing treatments.

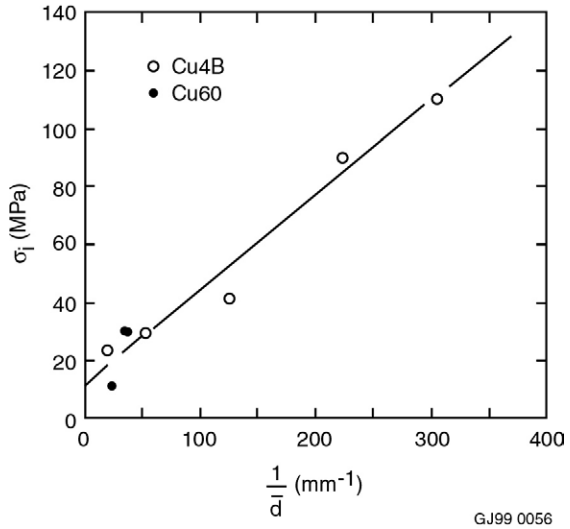

Figure 32. Apparent stress dependency on reciprocal grain size extrapolated from Stage II hardening.

The three stages represent in sequence: I—activation of boundary sources for dislocations; II—dislocation multiple cross glide (MCG);[9-11] and III—multiple cross glide in association with forest dislocation interactions. The rationale for these flow stress association with this sequential dislocation behavior is discussed below.

4.3.1 Stage I—Dislocation Source Activation

This transition region is associated with the onset of plastic flow and the corresponding deformations/strains have been referenced as those associated with micro yielding. The deformation/strain resolution from the tensile tests of this study were not sufficient to provide the microstrain correlations with stress as reported by others.[3–8] For five-nines polycrystalline copper, Bilello and Metzger[6] observe discernable grain size dependence over a plastic range from 0 to 0.0016. However, their finest grain size corresponded to the largest used in our study. The slopes for their flow stress-microstrain behavior appeared to be independent of the grain size and suggest that the grain size was only a factor for the onset of plastic flow. Bilello and Metzger[6] attributed the microstrain and influence from grain size to mobile dislocation segments having various threshold stresses for activation. The smaller the grain size the greater the activation stress for these mobile segments.

A later study by Malis and Tangri on polycrystalline copper focused on the microyielding region.[8] Grain boundaries and triple points were quite active in producing mobile dislocation segments at very low strains. Malis and Tangri argue that their observations support the interpretation that during the early stages of straining dislocation are predominantly emitted from the grain boundaries rather than being associated with impingement.

Several studies have addressed the flow stress behavior at small strains for polycrystalline nickel.[7,12] Lin and McLean[12] observed very significant dislocation populations at and in the near vicinity of the grain and twin boundaries at low strains. The authors concluded from their microstructural evidence that the boundaries could be either sources and/or sinks for dislocations. Malis, Lloyd, and Tangri[7] provided transmission electron microscopy (TEM) evidence for boundary emission of dislocations in prestrained polycrystalline nickel.

More recently, Varin, Kurzydlowski, and Tangri have proposed a model for grain boundaries as sources for dislocations.[13] Their model is based on extrinsic grain boundary dislocations, where the localized spreading of the dislocation core and the resulting consequences as stress concentrations appear to be the focal points of their arguments. They do make reference to gliding structural grain boundary dislocations (SGBDs) as potential dislocation sources, but such behavior would primarily be limited to twin boundaries. As a result metals that show propensities to form annealing twins (i.e., CSLs of $\Sigma 3^n$), the twin boundaries could prove to be a major source for lattice dislocations.

The results on polycrystalline copper show that the flow stress behavior at low strains, Stage I, is associated with the activation of dislocation sources. Furthermore, the apparent stress levels for activating these sources is inversely proportional to grain size as was shown in Figure 32.

A well known relationship exists between the average boundary intercept, $\bar{\ }$, and the boundary area (S_v) per unit volume of metal,[14] i.e.,

$$S_v = \frac{2}{=} \qquad (1)$$

The results shown in Table 6 suggest that the majority of the boundaries determined by OIM, and included in the boundary intercept measurements, are twin related boundaries, i.e., CSL - 3^n types.

TEM examinations were performed on foils from a prestrained (0.005) Cu4B copper tensile specimen given a 400°C anneal. Some representative TEM photomicrographs are shown in Figure 33. It is apparent from these photomicrographs that dislocations observed are primarily associated with the twin boundaries. As with most post-mortem examinations, one cannot unambiguously determine whether the twin boundaries are emitting or absorbing the dislocations. However, the evidence appears to favor emission over absorption. The dislocation population in the matrix appears to be very low; lower than what would be expected if the dislocations were coming from some other source. In a related manner, there should be more evidence of dislocation queues if absorption is occurring. The twin in Figure 33a shows dislocation half-loops along the twin boundary that would be more characteristic of dislocation multiplication. The twin boundaries shown in Figure 33b show two interesting features: (1) dislocations lying in the twin boundary and (2) a "wavy" character indicating that the boundary may be coming unstable. Additional examinations on prestrained copper specimens are needed.

4.3.2 Stage II—Dislocation Cross-Glide

The transition from Stage I to Stage II associated with flow stress observations leads to an increment in strain where Stage II is independent of grain size. As discussed in the previous section, the grain size influence appears to be only associated with the onset of plastic flow. Figures 31 and 32 provided an empirical description for Stage II in terms of its relationship to grain size, i.e.,

$$\sigma_{II} = \sigma_i + 286\ (\varepsilon_p)^{\frac{1}{2}} \tag{2}$$

where σ_i is the extrapolated intercept for Figure 30 and shown in Figure 31 as a function of the average reciprocal grain size that includes twins. Empirically, σ_i (in MPa) is

$$\sigma_i = 11.8 + 0.33\ d^{-1} \tag{3}$$

where the average grain diameter is in mm. The intercept correlation with just twin boundary surface area/unit volume, S_v, determined from the CSL $\Sigma 3^n$ orientations (see Table 6) is shown in Figure 34. These results can be empirically described (in MPa) by the following relation:

$$\sigma'_i = 14.2 + (2.27 \times 10^{-4})\ S_v \tag{4}$$

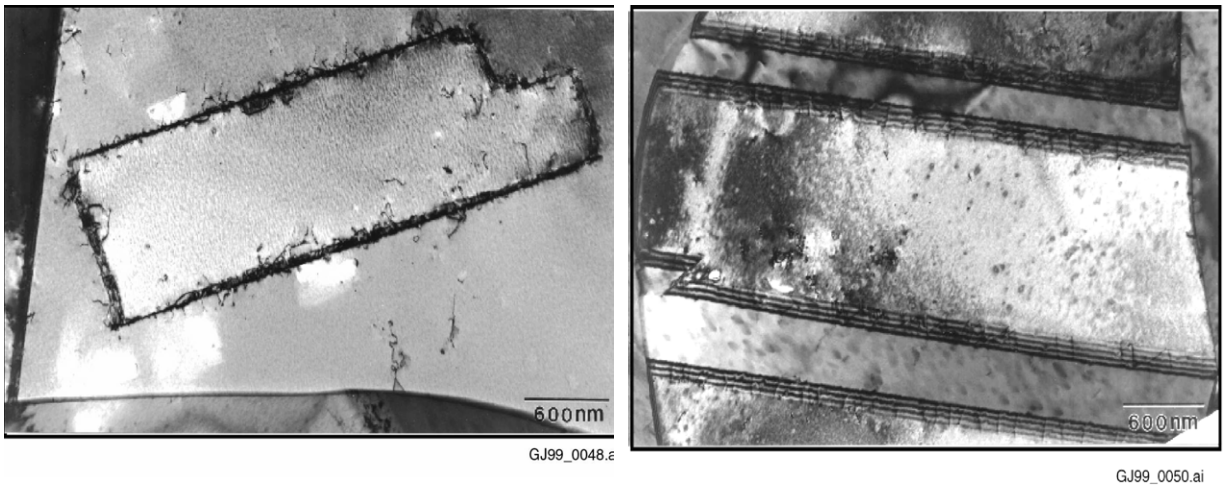

Figure 33. Exemplary twin regions in an annealed (400°C) Cu4B specimen after prestraining to 0.5%.

where S_v has units of m^2/m^3. The results shown in Figure 34 indicate that the two materials, Cu4B and Cu60, may reflect some influence from the cold working method after annealing to larger grain sizes.

The empirical descriptions of Equations 3 or 4 provide a form for normalizing the flow stress with respect to any dependency from grain size or twin boundary density. A $(\sigma_t - \sigma_I)$ or $(\sigma_f - \sigma_I')$ correction normalizes the flow stress behavior for both the Cu4B and Cu60 series. The linear portion of Stage II is interpreted as being associated with multiple-cross glide (MCG) of screw dislocations.[9-11] This process greatly increases the dislocation line length hence the dislocation density during straining. The relationship between strain and the dislocation density is given by

$$\rho = \rho_o + M\varepsilon_p \tag{5}$$

where ρ_o is the initial dislocation density, ρ is the instantaneous density, M is the multiplication coefficient for a polycrystalline material, and ε_p is the true plastic strain.[10,11] The extent of Stage II regions appears to transcend to Stage III after only a few percent strain (see Figure 30).

4.3.3 Stage III—MCG and Forest Strengthening

The Stage III strengthening is commonly interpreted as dislocation glide interaction with dislocation "threading" the glide planes. The "forest" model predicts the following relationship for the flow stress behavior:

$$\Delta\sigma_f = \alpha\mu b\,(\Delta\rho)^{1/2} \tag{6}$$

where α is a material constant that also includes a Taylor correction factor for polycrystalline behavior, μ is the shear modulus, b is the Burger's vector, and $\Delta\rho$ is the change in dislocation density from the onset of straining. Substituting Equation 5 into Equation 6, the following expression results:

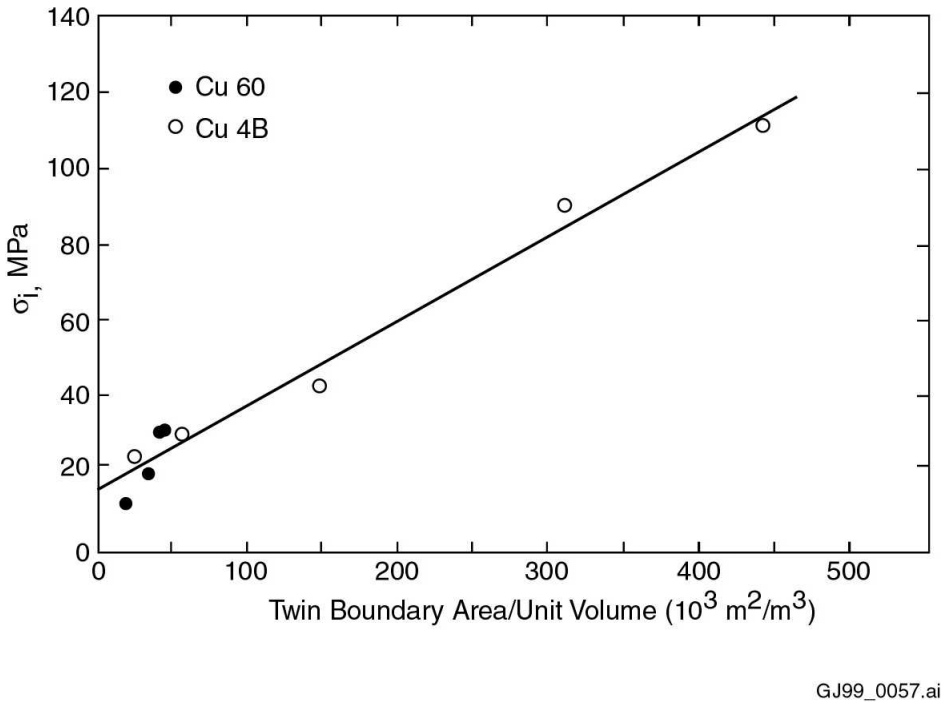

GJ99_0057.ai

Figure 34. Apparent stress dependency on the twin-boundary area/unit volume based on extrapolation from Stage II hardening.

$$\Delta \sigma_f = \alpha \mu b M^{1/2} (\varepsilon_p)^{1/2} \quad (7)$$

where the results for the copper series in Stage III, $\alpha\mu bM^{1/2}$ = 498 MPa. For copper, $\mu = 42\times10^3$MPa and $b = 2.56\times10^{-10}$m. Livingston has reported dislocation relations for stress and strain based on etch pit and TEM measurements[15] that confirm the relations (Equation 6 and 7) for copper. The value for M for polycrystalline copper is 2×10^{15} m^{-2} and includes a Taylor factor of 3.06 (i.e. average from Table 6). For α, Livingston determined a value of 1/3 for single crystal copper or 1.02 for polycrystalline copper. Using the latter, the $\alpha\mu b(M)^{1/2}$ term is calculated to be 490 MPa compared to the measured value of 498 MPa. Backtracking to Stage II, the same expression as Equation 7 would be expected to describe the flow stress behavior, except the α value would be reduced commensurate with the lower slope compared to Stage III, i.e., instead of 1.02, for Stage II the α value would be about 0.6 for polycrystalline copper.

For polycrystalline copper, the three stages of strain hardening are summarized as follows:

$\varepsilon_p < 0.002$—Stress activation of boundary sources for dislocations

$0.002 < \varepsilon_p < 0.01$—Dislocation multiple cross glide (MCG)

$\varepsilon_p > 0.02$—MCG plus dislocation forest hardening.

4.3.4 Annealing Twins—Dislocation Association

The observations from this study on copper strongly suggest that the twin boundaries are sources for dislocations. As these sources continue to operate during the straining process it is conceivable that the twins would "dissolve" with a gradual elimination of the lattice rotation associated with the twin itself. Geometrically this "dissolution" process is difficult to visualize particularly in terms of the emission of screw dislocations from these twin regions. Although not confirmed in this study, the dislocation population would be expected to be primarily Shockley-screw partial type dislocation, i.e., the a/6 <112> type since copper has a low stacking fault energy.

Orientation image microscopy (OIM) measurements on prestrained copper specimens are shown in Table 8. These results are consistent with the notation that as the twin regions continue to produce dislocations, eventually they could dissolve. Admittedly, arguments for the disappearance of the twin orientations through masking by subcell formation at higher strains cannot be discounted at this time. Further analysis is needed on this subject.

The observation that the twin boundaries may be the major source for dislocations in fcc metals poses an interesting concept. Could the dislocations, in a mechanistic sense, be recycling? The formation of twins on annealing for fcc metals appears to be a little vague. Prior to annealing, the microstructure,

Table 8. Orientation measurements on ECAE copper and Cu60 specimens after straining.

Specimen	True Strain	Fraction CSL-$\Sigma3^n$	Taylor Factor	Schmid Factor
Cu60	0	0.545	3.11	0.44
	1.1	0.087	3.07	0.432
Cu4C	0	0.67	3.00	0.44
	0.35	0.157	3.07	0.423

after significant amounts of cold working, show dislocation arrangements primarily as low angle grain boundaries in association with cell/subgrain development. Upon annealing, recovery and recrystallization processes change this cold work microstructure to the higher angle grain and twin boundaries (See Table 8). Meyers and Murr propose a nucleation and propagation model for annealing twin formation in fcc metals and alloys.[16] In their model, twin nucleates from a grain boundary and grows into the grain by the migration of a noncoherent twin boundary. The noncoherent twin boundary is represented by an array of Shockley partial dislocations whose total Burger's vector is equal to zero. It is not clear on how a significant portion of a grain can undergo the type of lattice rotation necessary for twin formation from this mechanism. The partial dislocations in very large numbers to form the cold work structure would need to thermally glide to the non-coherent twin boundary where they are absorbed causing the twin boundary to propagate and accompanied by the necessary lattice rotation of a significant portion of the grain. In other words, the partial screw dislocations may be coming back to reconstruct the twins by thermal glide during annealing. When formed, the twins upon the application of an applied stress start to "unzip," in a sense releasing the partial screw dislocations back to provide for the deformation, as well as the residual statistically stored and geometrically necessary dislocation population.[17] Further thought and analysis are needed in order to gain a complete understanding of annealing twin formation and their role as a primary source for dislocations.

4.4 Conclusions and Future Efforts

The flow stress results for the copper represent a major breakthrough in terms of true stress/true strain behavior for fcc metals. The ECAE copper provided material that would be difficult to obtain by other cold-working methods. This material had a very fine grain size after annealing, and the fine grain size proved instrumental in establishing the role of grain boundaries in strengthening. The findings on the flow stress behavior for polycrystalline copper will be submitted for journal publication. Additional ECAE metals—Al, Ni, and α-brass—are being prepared to confirm the generality of flow stress behavior of fcc metals.

5. ECAE PROCESSING OF ALUMINUM ALLOYS

5.1 Background

Current processing methods that are used to develop fine-grained superplastic microstructures in aluminum alloys involve extensive hot and cold deformation steps, usually in the form of hot and cold rolling. This approach has distinct limitations that can have a significant influence on the cost and quality of superplasticity-forming (SPF)-grade aluminum sheet. First, the extensive cold rolling required for SPF aluminum sheet typically results in substantial edge cracking and overall yield losses. The second limitation is that the high levels of hot and cold work necessary to achieve the desired microstructure requires starting with very large ingot size, while the final product is limited to thin sheet gage thickness.

The ECAE process offers several potential advantages in the processing of SPF-grade aluminum alloys. The ability of the ECAE process to achieve high levels of work through localized shearing can provide a mechanism for distributing the eutectic constituent particles and dispersoids that play a critical role in the recrystallization process and resulting thermally stable fine grain size. In addition, with ECAE there is the unique ability to achieve these desirable microstructures without reducing the dimensions of the starting material, as is the case in conventional processing of SPF materials.

Previous work performed on modified 5XXX-series alloys identified several compositional features that are necessary in developing the fine, thermally stable, grain structure required for SPF. One of the key features is the generation of an optimum distribution of coarse (1–5 μm) eutectic constituent (EC) particles combined with a uniform distribution of Al_6Mn dispersoid particles generally in the submicron size range.[18] This particle distribution, when combined with specific levels of cold work and recrystallization heat treatment, generates a very fine grain size (<10 um) that remains stable at typical SPF temperatures. Achieving the desired particle distribution and suitable levels of cold work requires that the 5XXX alloys contain minimum levels of Mn and to a lesser extent, Mg.[18] Mn is a very powerful dispersoid forming element in the 5XXX alloys (one Mn to six Al), and PNNL researchers believe that previous ECAE processing of Al5083 involved an alloy having a less than the critical level of Mn.

5.2 Materials Selection

There has been a lot of interest in aluminum 5083 alloy for SPF, due to its good strength, weldability and good corrosion resistance. Previous work performed at PNNL on modified 5XXX-series alloys identified several compositional features that are necessary in developing a microstructure that is advantageous to SPF. This previous work provided the basis for material alloy selection for ECAE processing to improve superplastic performance of 5XXX-series aluminum alloys. An aluminum 5083 alloy, with compositional modifications, was investigated for their enhanced superplastic behavior and thermal stability.

A total of four alloys were selected, one commercially available 5083 alloy, and three modified alloys that were previously direct cast by Kaiser Aluminum. All modified alloys had a base 5083 composition, with the iron and silicon impurities held to a minimum. In addition, two of the modified alloys had specific additions of zirconium and/or manganese to help create a fine, thermally stable microstructure. Table 9 lists the alloy identifications and compositions.

The 5083-com was an off-the-shelf commercial alloy, purchased in the form of a 1.25 inch hot-rolled plate in the H321 temper. This is the base-line chemistry to compare the effects of composition of the other alloys against. It represents the superplastic performance of a readily available commercial alloy processed by ECAE.

Table 9. Actual alloy compositions.

		Chemical Composition (w%)						
Identification	Alloy	Fe	Si	Mg	Mn	Cr	Zr	Ti
5083-com	Commercial 5083	0.40 max*	0.40 max*	4.0-4.9*	0.40-1.0*	0.05-0.25*	-	0.15 max*
Alloy 2	5083	0.08	0.04	4.89	0.81	0.19	0.05	0.03
Alloy 19	5083 + Mn	0.07	0.03	4.69	1.56	0.18	-	0.03
Alloy 20	5083 + Zr	0.08	0.03	4.76	1.59	0.19	0.20	0.03

a. Aluminum Association Compositional Range.

Alloy 2 had a nominal AA-5083 composition, in which the impurity levels were at a practical minimum for commercially producible castings. The lower impurity levels reduced the amount of Fe and Si containing constituents produced during solidification, hence limiting the large particles present that are ultimately initiation sites for cavitation during forming operations.

The remaining two alloys, 19 and 20, had 0.2% Zr and/or additional 0.8% Mn added to the high-purity 5083 alloy. During preheat treatment, fine Al_6Mn and Al_3Zr dispersoids ≤1 μm in size form. These fine particles slightly increase alloy strength, raise the recrystallization temperature and suppress grain growth, creating a structure that is thermally stable at forming temperatures.[18]

5.3 Preparation of Billets and ECAE Processing

All materials that were processed were extruded through the ECAE die obtained from Alcoa. Appropriate billet dimensions for this die were 31 mm square and approximately 152 mm long. Four billets of each alloy type were machined according to the dimensions above. Extra billets of pure aluminum were fabricated to aid Idaho National Engineering and Environmental Laboratory (INEEL) technicians in initial extrusion die setup and trial runs.

The 5083-com billets were annealed at 343°C for 1 h from the original H321 temper, to give an O-temper and strain-free starting condition prior to processing.

Past research work has shown that a homogenization of 500°C for a minimum of 4 h is optimum for modified 5083 alloys.[18] In addition, this preheat treatment produces maximum precipitation of fine Al_6Mn and Al_3Zr particles from solid solution. Alloys 2, 19, and 20 received such a preheat treatment prior to extrusion.

The purpose of deforming these materials through the ECAE process was to create a stable grain size of less than 10 μm. An initial batch of ECAE billets was sent to INEEL for processing through the Alcoa ECAE die setup. These billets were comprised of four 99.8% pure aluminum and four annealed 583-com billets. The pure aluminum billets were extruded through the Alcoa die multiple times at room temperature conditions without incident.

Initially, the 5083-com billets were to be extruded at room temperature. However, due to material strength, limited ductility at room temperature, and die capacity limits, it was determined that this extrusion condition was not possible with the available setup. Therefore, a series of elevated temperature

ECAE runs were attempted to determine the lowest possible extrusion temperature, without billet cracking. Multiple passes were successful at an extrusion temperature and rate of 250°C and 10 mm/min respectively. Only single passes were possible at extrusion temperatures of 150°C, with moderate billet cracking still occurring. Ultimately, two 5083 billets were processed at 250°C, one billet at 150°C and one billet at room temperature. The billets processed at 250°C were extruded through a total of four passes, one each via Routes B and C and are numbered A12-4B and A13-4C respectively. The other billets processed at room temperature and 150°C are numbered A10-1A and A11-4A respectively.

5.4 Microstructure Evaluation

Prior to, and after ECAE processing, microstructural examination was conducted on appropriate sections using optical microscopy (OM) and transmission electron microscopy (TEM). Microscopy was used to characterize grain size, degrees of strain, as well as identifying eutectic constituent size and distribution in the as cast and ECAE processed conditions.

Figures 35 and 36 show a comparison of eutectic constituent particle size and distribution, between the 5083-com material in an as-received and ECAE-processed condition. Following ECAE, the eutectic constituents have been broken up and are approximately one third to one fourth their original size, with good homogenous distribution throughout the matrix. These smaller well distributed eutectic constituents are advantageous to the development of a fine grain microstructure and therefore superplastic properties. The homogenous distribution of particles following ECAE indicates the potential of mixing or distributing particles in many different types of alloys or composite systems, in the solid form.

Though extrusion passes at room temperature conditions on the 5083-com materials were not successful without severe billet cracking, it was possible to obtain one pass through the die setup at a temperature of 150°C. Minor cracks occurred in the billet along the top edge (the face with the highest friction), but were not nearly as severe as the cracks following room temperature extrusion conditions. As shown in Figure 37, a high degree of cold work is present in the material, even after one pass. The TEM micrograph shows an elongated filament-like microstructure, with a high degree of strain. This type of structure is typical of ECAE Route A billet orientation during processing, and is not advantageous to superplastic properties. Even with a higher degree of cold work (after multiple passes through the extrusion die), the elongated microstructure would not recover/recrystallize to a fine grain equiaxed microstructure < 10 μm, at forming temperatures. Instead larger grains would develop, which are not desired for SPF.

It would seem that ECAE processing via Route C by nature of the billet orientation and therefore the alternating direction of strain, would generate the desired highly cold worked, fine equiaxed grain microstructure. In fact, in the literature this has been shown to be true .[18,19] Figure 38 shows a TEM micrograph of alloy 5083-com after ECAE processing at 250°C via Route C through a total of four passes. After four passes, prior to annealing, a well developed subgrain microstructure was established, with 200 nm to 1 μm grain size. The diffraction pattern of this area supports the fact that the microstructure is comprised of low-angle grain boundaries. The small dark areas are the Al_6Mn dispersoids particles, which are present to suppress grain growth at elevated temperatures.

In addition, the fine dispersoids seem to have an affect on subgrain size. From the TEM examination, the 5083-com material does not appear to have homogeneously distributed Al_6Mn particles, but rather has areas with high concentrations of particles. Figure 39 shows such an area, with a fine

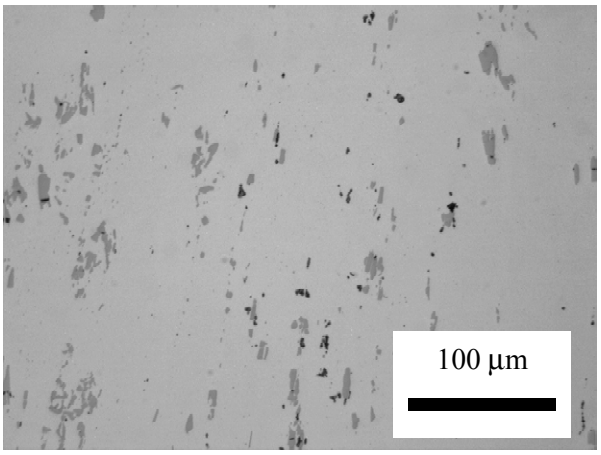

Figure 35. Optical photomicrograph of as-received 5083-com material.

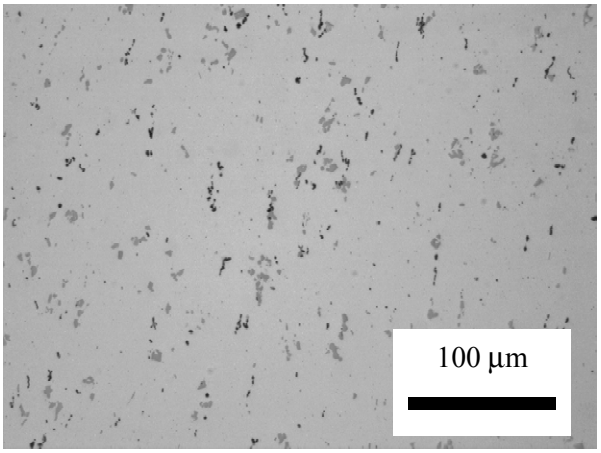

Figure 36. Optical photomicrograph of 5083-com material after ECAE (four passes, Route C).

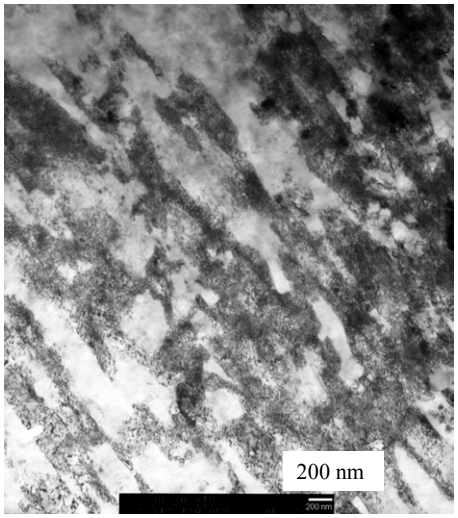

Figure 37. TEM photomicrograph of 5083-com material after ECAE (one pass, 150°C) showing the high degree of cold work.

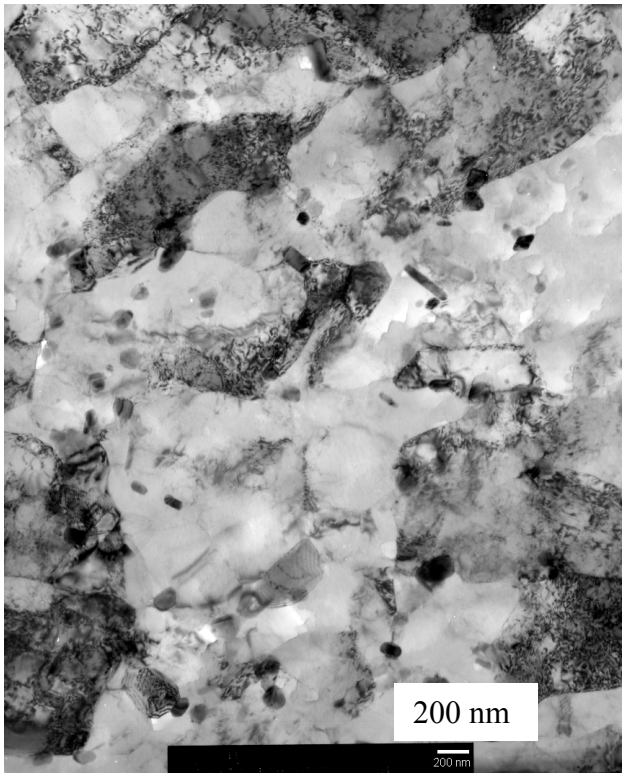

Figure 38. TEM photomicrograph of 5083-com material after ECAE (four passes at 250°C, Route C). The subgrain microstructure, on the order of 200 nm to 1 μm, is well developed.

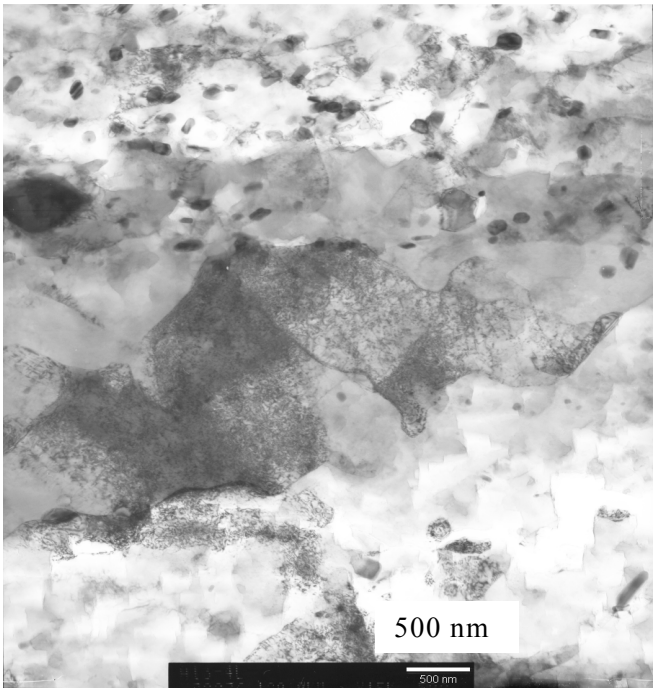

Figure 39. TEM photomicrograph of 5083-com material after ECAE (four passes at 250°C, Route C). Regions of fine equiaxed microstructure are associated with fine dispersoid particles.

equiaxed microstructure associated with the area of high dispersoid concentration. The adjacent area has an equiaxed microstructure also, but the grain size is approximately twice the size.

Random scans across the TEM microscopy sample of the 5083-com material extruded via Route C at 250°C and four passes reveled essentially the same well developed subgrain microstructure, but lacked significant areas with fine equiaxed grains with high-angle grain boundaries. However, there were small isolated areas that contained high-angle grain boundaries, with 500 nm to 1μm grain size. Figure 40 shows such an area, with well defined high-angle grain boundaries and moderate dislocation/subgrain structure, indicating that some degree of dynamic recrystallization is occurring during the ECAE processing at this temperature and strain rate.

5.5 Conclusion

Equal channel angular extrusion does induce a high degree of cold work, especially if the material is passed through the die multiple times. The extrusion processing was able to produce a fine equiaxed microstructure, in limited regions of the commercial 5083 material, with a grain size < 1μm. However, the vast majority of the processed billet did not have a well developed, equiaxed, high-angle grain boundary microstructure that is desired for SPF. Instead, the microstructure was comprised of a fine subgrain structure.

Due to processing problems (gross cracking), it was necessary to extrude the 5083-com material at elevated temperatures, on the order of 250°C. Initially, room temperature processing was tried, but severe cracking occurred. This may have been a limit of both the material and the die design. However, elevated extrusion temperatures proved to be beneficial in increasing the rate of dynamic recrystallization. Further extrusion passes (~6 total passes) at a processing temperature of 250°C, or at a slightly lower temperature of 200°C could produce the fine equiaxed microstructure that is desired throughout the entire billet.

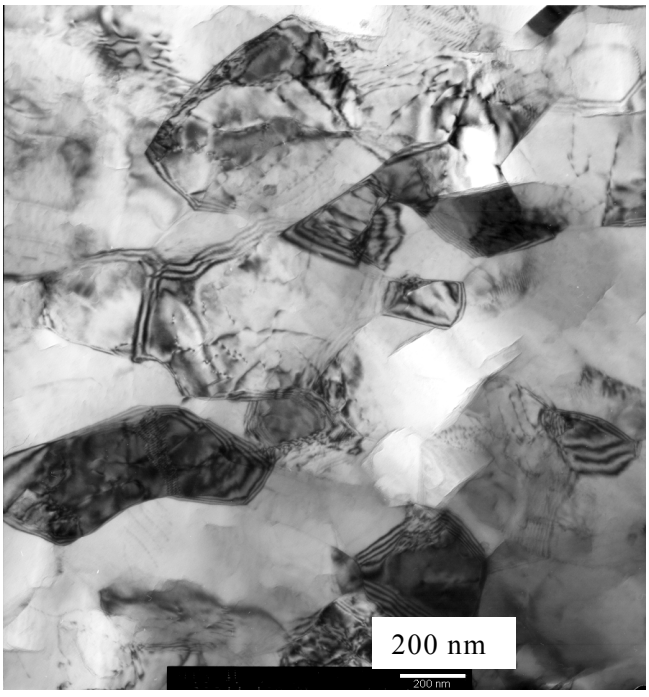

Figure 40. TEM photomicrograph of 5083-com material after ECAE (four passes at 250°C, Route C). Equiaxed fine grain microstructure, 500 nm to 1 μm, has high angle boundaries.

5.6 Summary of Future Work

Carry-on work for FY99 will include ECAE processing of the modified 5083 materials and further characterization. Microscopy examination will include orientation imaging microscopy (OIM) on current ECAE and future materials, as well as OIM, TEM, and limited scanning electron microscopy (SEM) on those materials to be processed.

In addition, hot hardness tests will be conducted to approximate the flow strength at various extrusion temperatures, in order to approximate extrusion loads and size tooling/billets accordingly.

After ECAE processing, the modified 5083 materials will be machined into SPF tensile testing specimens, to evaluate the superplastic properties and performance. Annealing studies on all materials will conducted also, to determine actual thermal stability to grain growth for varying processing parameters.

6. WELDING RESULTS

6.1 Resistance Spot Welding Electrode Test Summary

Resistance spot welding is widely used in the fabrication of vehicles for light and heavy-duty trucks. Major advantages of the process are high speed and suitability for automation and inclusion in high-production assembly lines with other fabricating operations. With automatic control of current, timing, and electrode force, sound spot welds can be produced consistently at high production rates and low unit labor costs by relatively unskilled workers.

Resistance spot welding is a process in which faying surfaces are joined in one or more spots by the heat generated by resistance to the flow of electric current through work pieces that are held together under force by electrodes. A short-time pulse of low-voltage, high-amperage current to form a fused nugget of weld metal heats the contacting surfaces in the region of current concentration. When the flow of current ceases, the electrode force is maintained while the weld metal rapidly cools and solidifies. The electrodes are retracted after each weld, which usually is completed in a fraction of a second.

Primarily the size and contour of the electrode faces limit the size and shape of the individually formed welds. The weld nugget forms at the faying surfaces shown in Figure 41 but does not extend completely through to the outer surfaces. In section, the nugget of a properly formed spot weld is round or oval in shape; in plan view, it has the same shape as the electrode face (which is usually round), and approximately the same size.

When welding certain materials, such as galvanized steel sheet, the spot welding electrode composition and type or configuration can affect on spot welding electrode degradation and spot weld consistency. In general, materials for spot welding electrodes should have sufficiently high electrical conductivity and sufficiently low contact resistance to prevent alloying of the electrode face. They should have adequate strength to resist deformation at operating pressures and temperatures. Because the electrode face contacts the workpiece during spot welding and becomes heated to high temperatures, hardness and annealing temperature must also be considered.

The purpose of this report is to summarize the status of the spot welding electrode development that was performed with electrodes that were made using the equal channel angular extrusion process. This work establishes baseline data for the degradation of nonalloyed equal channel angular extrusion (ECAE)copper spot welding electrodes and compares this baseline data against data generated with commercial and non-commercial electrodes. Degradation of the spot welding electrodes was determined by peel tests, axial microhardness, and scanning electron microscopy studies. The following presents the details of the spot welding tests and the initial results of these studies.

The tested electrode materials were CuCrZr, as-received Cu (Alloy C101 OFE - 99.99), AL-15 (Glidcop®), ECAE #4B, and ECAE #4C (electrode chemistries and processing details have been previously stated elsewhere in this report). The substrate materials used for the work were 0.8 mm-thick hot-dipped galvanized steel sheet. The material surface was cleaned or wiped with acetone prior to welding; no other special precautions were invoked. A Taylor-Winfield 150 kVA spot welder (Type IP-12-150) equipped with a Weldtronic/Technitron WT-500C micro processor control unit was used to weld spot welded coupons. Current was monitored with a WCT Weldcorder+ (Model MDDI-05A) Hall effect monitoring unit. The Electrode configuration used in this experiment was a 40° to 45° truncated cone male type electrode with a 6.3 mm face diameter. The welding schedule is given in Table 10.

Table 10. Developed welding schedule.

Condition	Parameter
Welding force	2270 N
Minimum nugget diameter	4 mm
Nominal nugget diameter	5 mm
Squeeze time	1.0 s
Welding time	0.2 s (`12 cycles)
Hold time	0.5 s
Welding Rate	~ 5 welds/min[a]

a. Estimated.

The experimental technique uses current levels that produce a 6.3 mm diameter spot weld nugget. To monitor welding behavior more precisely, numerous weldability tests were performed during the electrode life evaluation using the following sequence:

- 100 conditioning welds were made (electrode break-in)
- Peel tests were done at 200 weld intervals following break-in. Five peel tests were used to establish the average nugget size
- If sticking conditions were observed, they were recorded
- Termination of the electrode life test was established through the peel tests. The test was continued until a no-weld condition was found on three out of five peel tests coupons or if the number of samples exceeds 1,000.

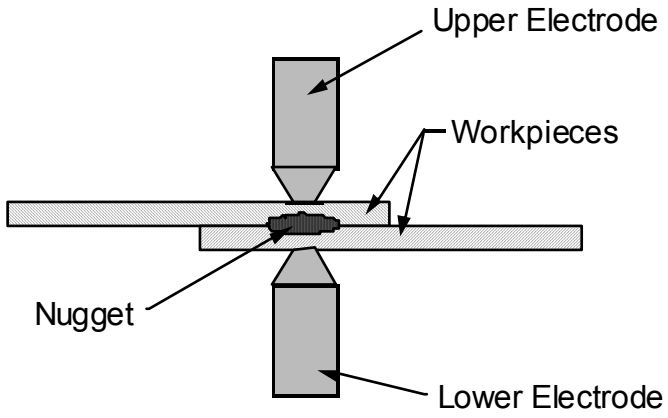

Figure 41. Arrangement of electrodes and workpieces in resistance spot welding. Note nugget relative to inner and outer surfaces of workpieces.

Figure 42 shows the results of the electrode degradation tests. These results indicate that the CuCrZr and AL-15 Glidcop electrodes had the longest longevity, followed by the as-received and ECAE copper electrodes. The CuCrZr and Glidcop electrodes degraded after approximately 900 welds, while the C101 copper electrodes degraded after approximately 500 spot welds. Degradation of the ECAE 4B and 4A/4C electrodes occurred after 300 and 100 spot welds, respectively.

Axial diamond pyramid microhardness tests were conducted on cross-sections of the electrode. The microhardness tests used a 500 g load with an interval of 0.5 mm (0.020 in.), and began at the tip and progressed inwardly to the unaffected electrode material. Results are shown in Figure 43. The as-received AL-60 Glidcop electrode was not used in the spot welding test and is used as a comparison standard for the results of the other electrodes. The AL-60 Glidcop electrode had as-received hardness of approximately 170 DPH. Hardness of the CuCrZr electrode showed unaffected material hardness equal to that of the AL-60 Glidcop; however, the tip (e.g., the first few mm) exhibited a hardness decrease to approximately 140 DPH. Similarly, the AL-15 Glidcop electrodes exhibited an unaffected material of approximately 135 DPH with a tip hardness decrease to a 125 DPH. Overall these electrodes showed hardness at least 2 to 3 times that of the ECAE and as-received Cu hardnesses. ECAE electrodes showed an approximate unaffected material hardness of 135 DPH with a tip hardness of 58 DPH. The softened tip region of the ECAE electrodes is much larger, approximately 7 mm (0.028 in.) as compared to the 0.5 mm (0.020 in.) zone of the CuCrZr and Glidcop electrodes. The as-received copper electrode exhibited a hardness between 58 DPH and 65 DPH. It should also be pointed out that the ECAE electrodes made about one-tenth to one-third the spot welds as did the CuCrZr and Glidcop electrodes before excessive degradation occurred. Measurements of the electrode face diameters after spot welding showed an inverse correlation between the hardness of the electrode tip and the deformation or dimetral increase of the electrode face. Given constant weld parameters, an increase in the electrode face diameter will decrease the current density of the welding at the faying surfaces of the galvanized sheet, thus decreasing the resultant size of the spot weld nugget.

Scanning electron microscope (SEM) photomicrographs were taken of the electrode tips of each material type. Energy dispersive spectroscopy was performed to determine if zinc is present in the electrode tip and if there was a gradient of zinc. A typical SEM photomicrograph, shown in Figure 44, indicates four different zones. Each of these zones has not been fully characterized; however, initial results indicate that the depth of the zones for each tests series (e.g., AL-15 Glidcop and CuCrZr) are different. Figure 45 shows the zone depth as a function of electrode material. The zone depths were measured from the SEM photomicrographs and indicate the depth or distance for each zone from the end of the electrode for each electrode material. Figure 46 shows three basic material types: oxygen-free copper (as received Cu and ECAE 4B), alloyed copper (CuCrZr), and dispersion–strengthened copper (AL-15 Glidcop). The data indicate that the CuCrZr electrode had the greatest depth of zinc penetration, followed by the oxygen-free copper and Glidcop electrodes. It should be pointed out that the CuCrZr and Glidcop electrodes were used to make approximately 900 welds, the as-received copper electrode was used to make approximately 500 welds, and the ECAE 4B electrode was used to make approximately 300 welds.

Figure 46 indicates the zinc concentration gradient for the various electrodes. The data indicate that the zinc concentrations through zones 1 and 2 are approximately equal for the Glidcop, as received and ECAE 4B electrodes; however, the CuCrZr electrode showed a significant decrease in the zinc concentration gradient at the end of the electrode.

Spot welding electrodes perform three purposes: (1) to conduct welding current to the work and determine current density in the weld zone, (2) to transmit force to the workpiece, and (3) to dissipate heat from the weld thus thermally constraining the nugget. If the application of pressure were not involved,

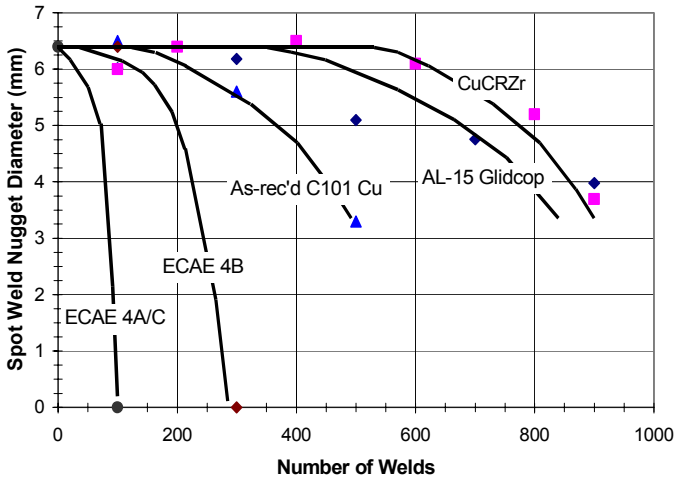

Figure 42. Electrode degradation tests show a dependency on materials.

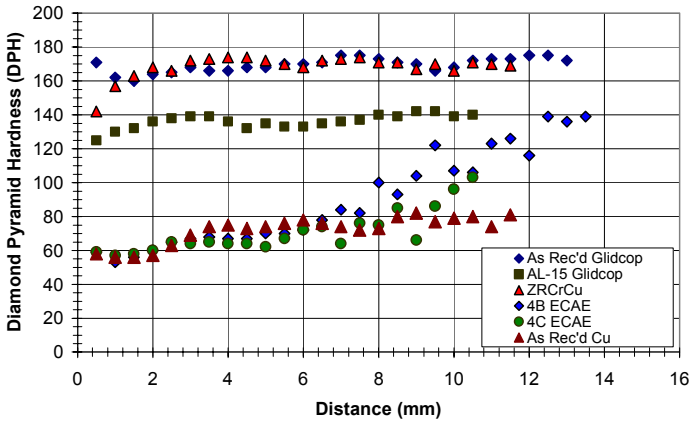

Figure 43. Axial hardness traverses of spot welding.

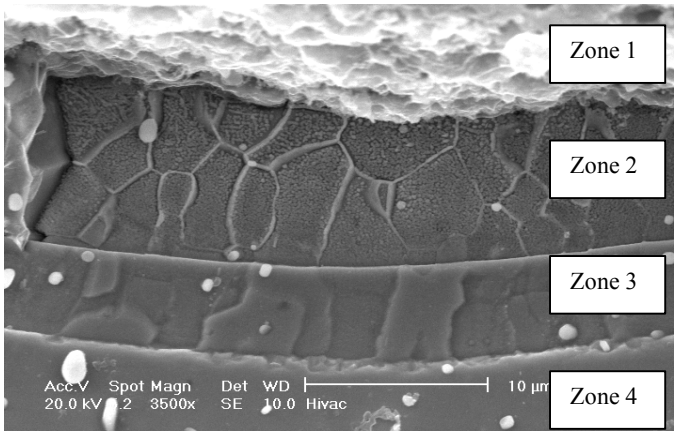

Figure 44. Scanning electron microscope photomicrograph of the tip of a CuCrZr electrode. The specimen has experienced 900 spot welds on.

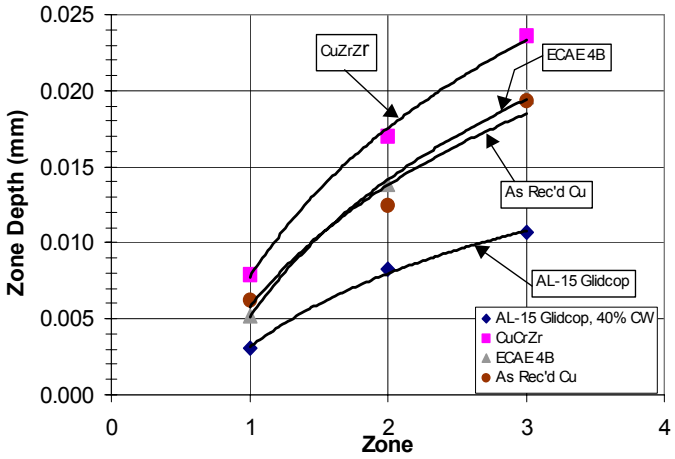

Figure 45. Variation of zone depth for the different electrode material.

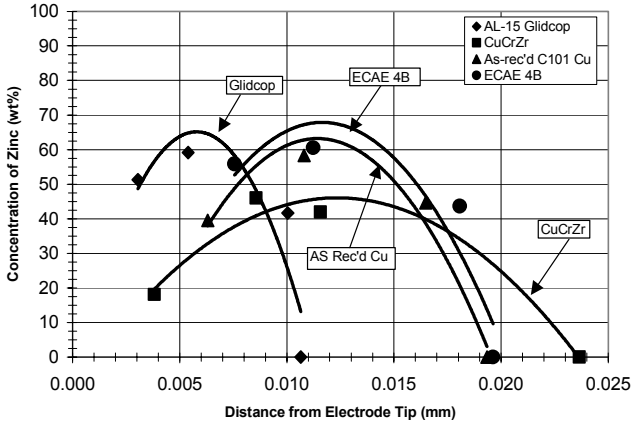

Figure 46. Concentration of zinc as a function of distance form the end of the electrode tip.

electrodes could be selected almost entirely on the basis of electrical and thermal conductivity. Since electrodes are subjected to forces of considerable magnitude during spot welding, they must be capable of withstanding the imposed stresses at elevated temperatures without deformation. Proper electrode shape is important because current must be confined to a locally fixed area to achieve needed current density to form an acceptable spot weld.

6.2 Future Work

Equal channel angular extrusion was seen as a processing technique that would increase yield strength and hardness and thus limit deformation while maintaining electrical conductivity. The above results indicate that ECAE-processed commercially pure copper electrodes are not a good choice for electrodes. As a result of recrystallization, hardness of the ECAE electrodes decreased to that of the as received copper after a few spot welds or thermal cycles. Further tests to evaluate ECAE effects on spot welding electrode materials are planned and will be conducted with more thermally stable materials such as alloyed and dispersion-strengthened copper (e.g. CuCrZr and Glidcop, respectively).

7. NANOCRYSTALLINE COPPER-AL_2O_3 ALLOYS PREPARED BY EQUAL CHANNEL ANGULAR EXTRUSION

7.1 Background

Oxide-dispersion-strengthened (ODS) copper, commercially available under the trade name Glidcop^{TM}, is used for tips of welding electrodes. A microstructural examination of this alloy reveals that some of the oxide particles providing the hardening are large and unevenly dispersed throughout the copper matrix. We believe that by using ECAE, one can obtain an alloy having finer and better dispersed oxide particles. This should result in greatly improved high temperature mechanical properties (hardness, creep resistance).

The welding tip material is subjected to a large compressive stress and, at the same time, the passage of large current pulses. Although the body of the tip is water-cooled, the surface where the tip makes contact with the material being welded experiences large periodic temperature increases. The combination of an applied compressive stress and high temperature pulses causes plastic deformation of the tip (blunting), increasing the welding contact area. In turn, an increase in the welding contact area results in a decrease in the *current density*, and this conduces to a poor weld of low mechanical strength.

The problem at hand is therefore the development of a high-electrical- and high-thermal-conductivity alloy that retains high mechanical strength at high temperatures. Since the tip must be cheap, and must have high electrical and thermal conductivity, the material of choice is a fine-grain dispersion-strengthened copper alloy. Two classes of dispersoids are being investigated: (1) intermetallics (such as Cr-Zr) and (2) oxides (such as Al_2O_3, and possibly MgO).

In general, dispersion strengthening is effective at temperatures below $T_m/2$, where T_m is the melting temperature of the matrix. Below this temperature, the dislocations are unable to bypass the particles. Then, plastic deformation requires additional dislocation generation. This is the main contribution to the hardening, which adds to that strengthening provided by the grain refinement. The flow stress is then well described by the Orowan equation, $\sigma = \mu b/L$, where μ is the shear modulus and L is the mean separation between the dispersoids. Above $T_m/2$, dispersion strengthening looses its effectiveness because the dislocations can circumvent the particles by diffusion-assisted climb. This results in an increasing rate of creep with increasing temperature. However, if the hardening particles are copious and extremely small (on the nanometer range), and have an elastic modulus different from that of the matrix, then there is an additional hardening mechanism: due to the difference in modulus, there is an attractive elastic interaction between the dislocations and the particles, which prevents the dislocations from leaving the vicinity of the particles. This results in a hardening mechanism that operates at all temperatures. This mechanism, and the requirements for its operation, were described in the research proposal.[20]

7.2 Synthesis of ODS Copper by ECAE

The goal of this work is to develop a creep-resistant ODS copper alloy for use as tips of welding rods. Ideally, the alloy must posses the following characteristics:[1]

- Copper matrix with submicron size grains
- Copper grains elongated in the compressive/tensile direction (texture)
- Uniform dispersion of nanosized oxides both at grain boundaries and inside the grains

- Oxide dispersions must be stable at the maximum intended use temperature.

To prepare a copper-based alloy with these characteristics, we are using a combination of mechanical alloying and ECAE.

This work has the following components:

- *Synthesis of copper powders containing a homogeneous dispersion of nanosized Al_2O_3 particles:* The starting Cu powder is annealed in an argon/hydrogen gas mixture to remove adsorbed water and reduce any oxygen dissolved in the copper. The reduced Cu powder is then mechanically alloyed with aluminum powder to produce a homogeneous Cu(Al) solid solution. Then, the Cu(Al) solid solution powder is mechanically alloyed for a short time with CuO_x powder. At this stage, the powder product consists of a two-phase mixture of Cu(Al) and CuO particles. The Al_2O_3 reinforcing particles will not form until annealing at about 500°C, *after* the ECAE extrusion (see below).

- *Preparation of specimens for ECAE tests*: The powder consolidation via ECAE is done in sealed cans, with outside dimensions of 0.88"×0.88"×4.5". The powder is contained inside an axial ½-inch diameter by 3.5-inch long cavity. These cavities are sealed with tight fitting plugs of the same material as the can. Before loading the cans with powder, they are chemically cleaned. The powder loading is done inside a glovebox containing recirculated argon gas with less than 1 ppm oxygen. The powder density is maximized by vibrating the loaded cans while inside the glovebox, using a vibratory table specially constructed for this purpose. The cans are then evacuated and the lids are e-beam welded under vacuum. The sealed cans are then shipped to INEL for the ECAE extrusions.

- *ECAE extrusions*: The extrusions will be done at varying temperatures (starting at 300°C), and varying extrusion rates. We will also investigate the effects of the number of ECAE passes and type of pas (e.g., rotation of the sample between passes) on the microstructure of the product.

- *Post Anneal treatments*: We have determined (see following sections) that the optimum temperature for the development of nanosized Al_2O_3 particles is about 500°C. Since at present the ECAE die can only be heated up to 300°C, the extruded alloy will not have the desired microstructure. The Al_2O_3 precipitates will be formed during a post extrusion anneal treatment, where the aluminum atoms in the Cu(Al) solution will react with the CuO particles to form nanosized Al_2O_3 particles according to the reaction:

$$3CuO + 2Al \rightarrow 3Cu + Al_2O_3 \qquad (8)$$

- *Microstructural characterization:* We will use x-ray diffraction, optical and electron microscopy, electrical and thermal conductivity, and hot-hardness testing to characterize the microstructure and mechanical properties of the alloys. The integral breath method applied to the x-ray patterns will be used to measure the grain size and residual strains. These results will be corroborated by TEM. A hot-hardness indentor (Nikon) will be used to measure the high-temperature creep behavior of the extruded Al-Al_2O_3 alloys.

- Welding tips prepared from the ECAE extruded material will be tested at INEL in welding machines similar to those used by industry. The lifetime of the tips will be compared to those of commercial tips. Used tips (from commercial as well as ECAE-extruded material) will be sent to LANL for sectioning and examination via scanning electron microscopy.

7.3 Accomplishments (FY1999)

The starting commercial Cu powder was annealed in Ar-6 wt% H_2 atmosphere to reduce the copper oxide inclusions (surface and bulk). Figure 47 shows the thermo-gravimetric (TGA) trace obtained during the reduction anneal. The *change* in sample weight was monitored while the temperature was increased from 25 to 580°C. The copper powder looses weight in distinct stages, labeled A, B, and C. We attribute stage A to loss of adsorbed water; stage B to reduction of surface oxides; and stage C (starting at about 370°C) to reduction of bulk oxygen. These results enabled us to select the optimum temperature for cleaning the Cu powder prior to the mechanical alloying with aluminum.

A set of mechanical alloying (MA) experiments was performed on a Cu-10 wt% Al alloy to determine the optimum milling time required to alloy Cu and Al. For these tests, the aluminum addition, 10 wt%, was higher than what we will use to manufacturing welding electrode tips. This high aluminum concentration was chosen to make it simple to monitor the degree of alloying as a function of milling time using x-ray diffraction (XRD). Milling was performed using hexane (C_6H_{14}) as a dispersion agent. Samples were taken after milling times of 2 minutes, and 2, 4, 9, 12, and 23 hours. Figure 48 shows the XRD pattern after 9 h of milling. According to data from Pearson's Handbook of Lattice Spacings, the lattice parameter of copper increases at the rate of 5.27E-4 nm per wt% aluminum in solution. From the measured change in lattice parameter we determined that most of the aluminum goes in solution into the copper within four hours of milling. This optimum milling time was used to prepare various dilute Cu(Al) solid solutions, containing the amount of Al needed to make an ODS copper alloy having between 1 and 2 wt% Al_2O_3.

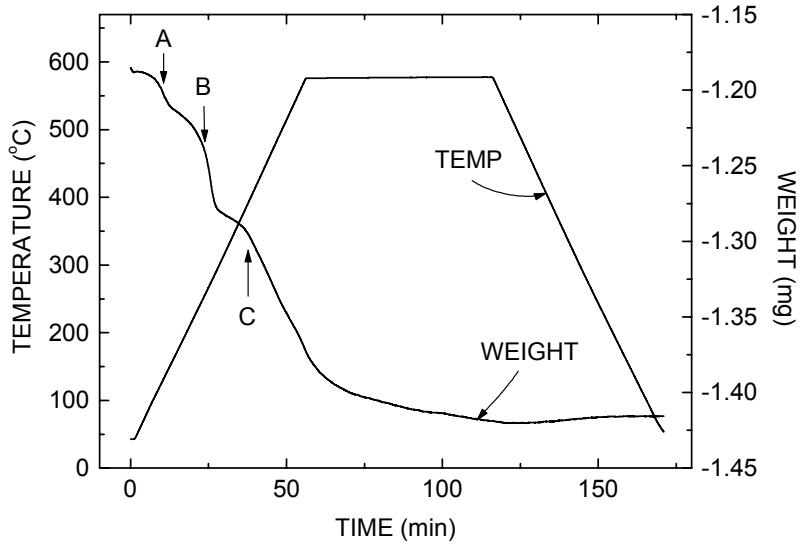

Figure 47. Thermo-gravimetric analysis of the reduction of commercial copper oxide powder.

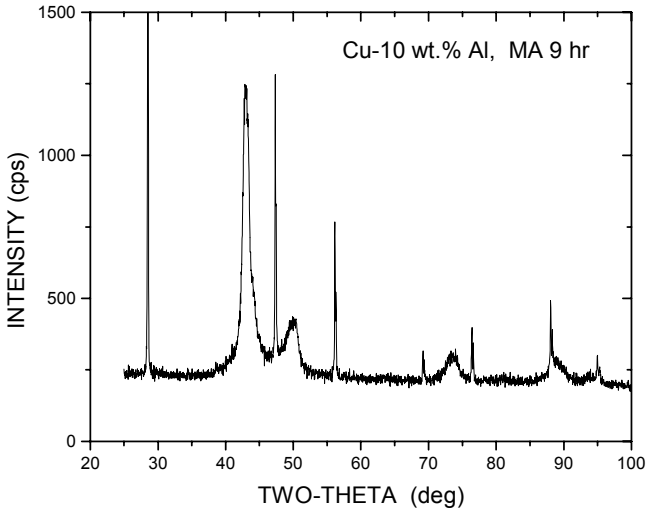

Figure 48. X-ray diffraction pattern of Cu-10 wt% Al mechanically alloyed for 9 h in hexane. The sharp Bragg peaks are from silicon powder (NIST standard) added to calibrate the abscissa. The broad Bragg peaks are from the Cu(Al) solid solution.

Having formed the Cu(Al) solid solution by ball milling, the next research step was to determine the diffusion kinetics of Al in the mechanically alloyed Cu(Al) matrix. We obtained this data from TGA tests. The mechanically alloyed Cu(Al) powder was heated to 700°C at the rate of 10 K/min, and was kept at that temperature for 1 h. The test was done in an Ar-6 wt% H_2 gas mixture flowing at 20 cc/min. The DTA trace is shown in Figure 49.

On heating up to about 480°C, the sample looses weight because the CuO formed on the surface of the powder (during the loading of the powder into the TGA machine, the powder is necessarily exposed to air) is reduced by the Ar-6 wt% H_2 gas mixture. However, when the temperature is increased above about 480°C, the powder begins gaining weight. This is due to the oxidation of the aluminum, which cannot be

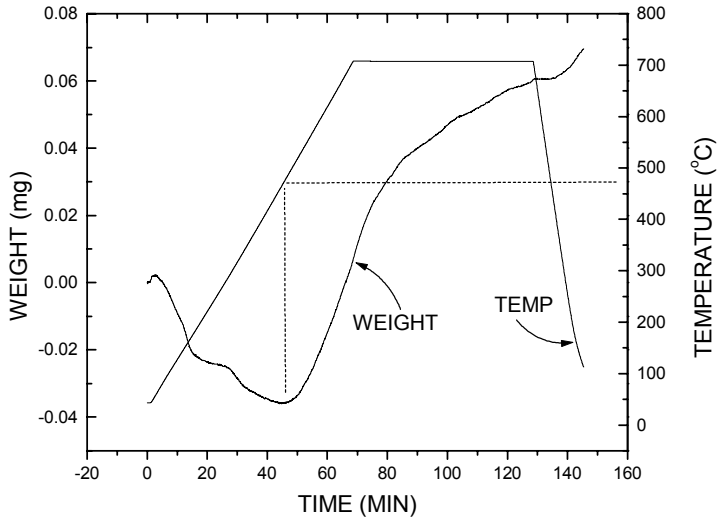

Figure 49. Temperature and weight-change in Cu-10 wt% Al solid solution annealed in Ar + 6 wt% H_2.

reduced by the Ar-6 wt% H_2 gas. Instead, oxygen or water impurities in the circulating gas are reduced by the aluminum, forming Al_2O_3. It is important to notice that the powder gains weight even when the temperature is maintained at the constant value of 700°C. This can only be explained by the *diffusion* of additional aluminum to the surface of the particles. Since the aluminum solutes in the Cu(Al) solid solution become mobile at about 500°C, the reaction:

$$Cu(Al) + CuO \rightarrow Cu + Al_2O_3 \tag{9}$$

leading to the formation of the ODS copper alloy requires an annealing temperature of at least 500°C.

The purpose of the ECAE extrusion is to produce a fully dense compact while maintaining the ultra-fine microstructure developed by mechanical alloying. In separate experiments conducted at LANL, we prepared Cu-Al_2O_3 powder by ball milling a mixture of Cu, Al, and CuO powders for 10 h. After this long-duration mechanical alloying, the aluminum and the oxygen in the CuO had already reacted to form Al_2O_3. The Cu matrix in the as-prepared powder had grain sizes on the order of 10 nm, as revealed by x-ray diffraction. Most likely, the Al_2O_3 inclusions were also small, but could not to be resolved by x-ray diffraction. We attempted to consolidate the Cu-Al_2O_3 powder by hot pressing it in a ceramic die at 700°C and at a pressure of 67 MPa. We found that due to its high hardness, and the retention of hardness at elevated temperatures, this powder did not densify. This suggests that the ECAE densification should be done on the Cu(Al) + CuO powder, *before* the Al_2O_3 has been formed, and while the aluminum is still in the Cu(Al) solid solution. The TGA results discussed above indicate that this is possible as long as the temperature during the ECAE process is kept below about 450°C. Then, after the powder has been consolidated by ECAE, the hardness of the alloy can be increased by a post-extrusion anneal in the vicinity of 500°C, which will enable the formation of the Al_2O_3 precipitates according to Equation 9.

Controlling the maximum temperature, T_{max},, reached by the material during the ECAE processing will require careful consideration of the energy dissipated during the extrusion. Assuming that the densification is adiabatic, we can derive an upper limit for the maximum temperature from the energy-conservation equation:

$$\sigma_{EXTR} = \int_{T_o}^{T_{max}} \rho \, C_p \, dT \tag{10}$$

where σ_{EXTR} is the applied extrusion stress, T_o is the initial die and billet temperature, and C_p and ρ are the specific heat and the density of the billet material. Assuming further that the specific heat and the density are independent of temperature, one obtains,

$$T_{max} - T_o = \sigma_{EXTR} / (\rho \, C_p) \tag{11}$$

The extrusion stress, σ_{EXTR}, depends on the material and its strain history. For the first ECAE pass, $\sigma_{EXTR} \approx 1.4 \, \sigma_{YIELD}$.[21] Typically, for copper, σ_{EXTR} for the first ECAE pass is about 70 ksi = 543 MPa. With this value, and the density and specific heat of copper, Equation 11 predicts a temperature increase of about 150 K. Thus, if the initial billet temperature is T_o = 300°C, during the ECAE extrusion the billet may reach a temperature of T_{max} = 450°C, which is below the temperature at which the aluminum starts to diffuse in the copper matrix. Thus, the above analysis shows that the optimum temperature for the ECAE extrusion is about 300°C.

7.4 Work in Progress

We have prepared several square cans for ECAE extrusion tests. Initially, we planned to use copper cans. We have now opted for aluminum cans for two reasons: (a) it will enable lowering the extrusion stress; and (b) it will enable a simpler analysis of the ECAE mechanism since the delineation between the consolidated copper powder and the Al can will be easier to distinguish by optical microscopy or by SEM. Three aluminum cans were loaded and sealed with the following powders:

1. Cu-1.1 wt% Al solid solution + 2 wt% CuO.

2. Mixture of spherical copper and silver powders, both -325 mesh.

3. Ti 15 wt% Mg powder prepared by mechanical alloying

These cans have been sent to the INEEL. Can 1 will be extruded at 300°C. It will produce a Cu(Al) + CuO bar having submicron grain sizes. A post anneal will enable the formation of the Cu + Al_2O_3 solid, as discussed above.

Can 2 will be extruded at room temperature. The mixture of spherical Cu and Ag powder will enable us to study the deformation of the powder particles during the ECAE extrusion. After the ECAE consolidation (1 pass only), the sample will be sectioned for a SEM study of the extrusion strain. In particular, we will determine the degree of particle elongation, indications of cold welding between adjacent particles, residual porosity, etc. Copper and silver are mutually insoluble and thus the Cu/Ag interfaces will remain sharp. This morphology study will be correlated with x-ray texture analysis measurements on this and other copper samples.

Can 3 will be extruded at 300°C. This is an *exploratory* test aiming at producing a high-strength/low-density alloy. Magnesium is slightly soluble in titanium (less than 1 wt% at 600°C). By mechanical allying we have produced a homogeneous hcp Ti-15 wt% solid solution having nanosized crystalline domains. The XRD pattern for this powder is shown in Figure 50. We expect that the ECAE consolidation will retain the fcc metastable structure of the starting powder. We will then study the mechanical properties of the compacted solid.

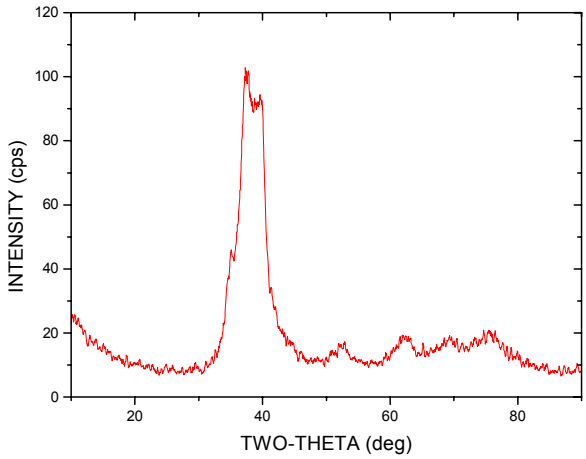

Figure 50. X-ray diffraction pattern for Ti-15 wt% Mg solid solution prepared by mechanical alloying.

8. FUTURE WORK

Work Scope below outlines the plan for continuing the investigation in FY99.

1. The study of copper will be completed. The following results will be summarized:

   - Microstructural evolution as a function of the processing routes and temperature stability of the produced microstructures
   - Effect of processing and heat treatment on mechanical properties of extruded materials
   - Flow stress analysis of copper: description of the stress vs. strain behavior based on the initial microstructural features such as grain size and fraction of special grain boundaries
   - Investigation of the nucleation and evolution of special grain boundaries, i.e., twins, as a result of ECAE deformation and annealing.

2. Investigation of the welding behavior of the ECAE processed copper and commercial spot welding electrodes will be completed. The following results will be summarized:

   - Electrode life assessment
   - Electrode cross-section analysis for hardiness and Zn diffusion
   - Effect of Zn presence in the coating of steels presence on electrode life performance.

3. Investigation of welding behavior of ECAE processed commercial Glidcop and CuCrZr electrodes.

4. Investigation of annealing twin formation and flow stress behavior in ECAE processed Ni, Al, brass, and stainless steels.

5. Consolidation of various powders (including nickel aluminides and amorphous powders) via ECAE processing.

6. ECAE processing of aluminum alloys for automotive applications.

7. Assessment of modeling needs/requirements.

9. REFERENCES

1. V. M. Segal, V. I. Reznikov, A. E. Drobyshevkiy, and V. I. Kopylov, Russian Metallurgy, Vol. 1, pp. 99–105, 1981.

2. S. Ferrasse, V. M. Segal, T. Hartwig, R. E. Goforth, "Microstructure and Properties of Copper and Aluminum Alloy 3003 Worked by Equal Channel Angular Extrusion," Metallurgical and Materials Transactions A, vol. 28A, April 1997.

3. D. A. Thomas and B. L. Averbach, *Acta Metall.*, 7, pp. 69–75, 1959.

4. N. Brown and K. F. Lukens, Jr., *Acta Metall.*, 9, pp. 106–111, 1961.

5. R. F. Tinder and J. Washburn, *Acta Metall.*, 12, p. 129, 1964.

6. J. C. Bilello and M. Metzger, *Trans. Met.*, 245, pp. 2,279–2,284, 1969.

7. T. Malis, D. J. Lloyd , and K. Tangri, *Phys. Stat., Sol(a)* 11, pp. 275–286, 1972.

8. T. Malis and K. Tangri, *Acta Metall.*, 27, pp. 25–32, 1979.

9. J. S. Koehler, *Phys. Rev.*, 86, p. 52, 1952.

10. J. J. Gilman, *J. Appl. Phys., 36, p. 2,772, 1965*.

11. J. J. Gilman, *Micromechanics of Flow in Solids*, McGraw-Hill Book Co., pp. 185–199, 1969.

12. T. L. Lin and D. Mclean, *Metal Sci. Journ., 2*, pp. 108–113, 1968.

13. R. A. Varin, K. J. Kurzydlowski, and K. Tangri, *Mater. Sci. and Eng., 85*, pp. 115–126, 1987.

14. C. S. Smith and L. Guttman, *Trans. AIME*, 197, p. 81, 1953.

15. J. D. Livingston, *Acta Metall.*, 10, pp. 229–239, 1962.

16. M. A. Meyers and L. E. Murr, *Acta Metall., 26*, pp. 951–962, 1978.

17. M. F. Ashby, *Phil. Mag., 21*, p. 399, 1970.

18. C. A. Lavender, J. S. Vetrano, M. T. Smith, S. M. Bruemmer, "Development of Superplasticity in 5083 Aluminum with Additions of Mn and Zr," Superplasticity in Advanced Materials: Icsam-94 (Materials Science Forum, Vol. 170-172), Terence G. Langdon, pp. 279-285, (1995).

19. V. M. Segal, "Materials Processing by Simple Shear," Materials Science and Engineering, 1995, pp. 157–164.

20. R. B. Schwarz, Research Proposal to DOE/OTT titled "Nanocrystalline Copper-Al_2O_3 Alloys Prepared by Equal Channel Angular Extrusion", April 6, 1998.

21. V. Segal, personal communication to Jenya Macheret (1999).